Electronic Supplementary Material (ESI) for Journal of Materials Chemistry A.

Supporting Information

HER/OER Mechanistic Study of FeCoNi-Based Electrocatalyst for Alkaline Water Splitting

Fu-Te Tsai,[†,*] Yu-Ting Deng,[†] Chih-Wen Pao,[§] Jeng-Lung Chen,[§] Jyh-Fu Lee[§], Kuan-Ting Lai,[‡]and Wen-Feng Liaw[†,*]

[†]Department of Chemistry and Frontier Research Center of Fundamental and Applied Science of Matters, National Tsing Hua University, Hsinchu 30013, Taiwan

[§]National Synchrotron Radiation Research Center, Hsinchu, Taiwan

[‡]Chemical Systems Research Division, National Chung-Shan Institute of Science and Technology, Taoyuan 325, Taiwan

Experimental Section

Chemicals. $FeSO_4 \cdot 6H_2O$, $CoSO_4 \cdot 6H_2O$, $NiSO_4 \cdot 6H_2O$ (Alfa Aesar), $NaNO_3$ (Aldrich), 99.9% IrO_2 powder, Nafion® perfluorinated resin solution (5 wt. % in lower aliphatic alcohols and water, contains 15-20% water) (Sigma-Aldrich), platinum disk electrode (surface area = 0.0707 cm^2) (ALS), glassy carbon disk electrode (surface area = 0.0707 cm^2, CH Instruments), graphite plate (R8340, 50×4×1 mm, Great Carbon Co., Ltd., Taiwan) and Ni foam (surface density 350 g/m^2, MTI corporation) were used as received.

Material Characterization. SEM images and EDX spectra were collected by a field emission scanning electron microscopy (JSM-6330F, JEOL Co. Ltd., Japan) operating at an accelerating voltage of 10 kV equipped with energy dispersive X-ray spectroscopy (Oxford). Powder X-ray diffraction (pXRD) data were obtained using a Bruker D8 X-ray Powder Diffractometer with a Cu Kα radiation source in the range 2θ = 10-70°. Infrared spectrum of electrodeposited film was recorded on a PerkinElmer model spectrum one B spectrophotometer with KBr solid. X-ray photoelectron spectroscopy (XPS) analyses were performed with a Phi Quanterall (Ulvac-Phi. Inc) using a high-resolution monochromatic Al Kα line X-ray source (1486.6 eV) and 200 μm spot size on the surface of the sample. The X-ray source was directed 45° with respect to the sample surface. The analyzer is located perpendicular to the sample surface. The spectra were registered at a base pressure of $< 5\times10^{-9}$ torr. The electron energy analyzer was operated with pass energy of 55 eV with 30 sweeps enabling high resolution of the spectra to be obtained. Because oxygen is always present on samples surface exposed to the atmosphere, either due to adventitious nitrate, phosphate or water, it is difficult to accurately quantify the oxygen content in these samples without argon ion sputter cleaning.[1-2] All XPS spectra were calibrated by referring carbon 1s peak at 284.8 eV. XPS peaks were assigned using MultiPak Spectrum software and Perkin-Elmer Handbook of X-ray Photoelectron Spectroscopy.[3] XPS data analysis and the peak deconvolution by using Gaussian−Lorentzian curve fitting based on Shirley background correction was accomplished with OriginPro 2016 software.

Electrochemical Measurements. Electrochemical measurements were carried out using a CHI model 621b (CH Instrument) potentiostat instrumentation with a standard three-electrode system. The graphite plates (surface area = 0.08 cm^2) were used as working electrode and auxilary electrode, respectively. The Ni foam (surface area = 0.08 cm^2) was used for the fabrication of CFeCoNiP/NF working electrode. SCE (saturated calomel electrode, pH = 7) and Hg/HgO (pH =14) were used as reference electrodes. The working

electrodes CFeP, CCoP, CNiP, CFeCoP, CFeNiP, CcoNiP, CfeCoNiP and CFeCoNiP/NF were prepared from electrochemical deposition of the corresponding metal sulfate(s) in 1 M phosphate buffer (pH = 7) under N_2 atmosphere onto the graphite plates or Ni foam using a gas-tight, two-compartment cell with *iR* compensation. The cathodic deposition process is based on the reduction of nitrate to ammonium cation along with the generation of hydroxide that could facilitate the depositon of metal oxide on the electrode surface.[9] Electrodeposition was accomplished by applying -1.0 V at 40 ^{o}C until the current density reaches an asymptotic limit (about 3 h). Films characterized *ex situ* prior to further electrochemical measurements are referred to "as-prepared" electrodes. Polarization curves of "as-prepared" electrodes in 1 M NaOH electrolyte were recorded by sweeping the potential from 0.00 V to -0.80 V and from 1.20 V to 2.00 V for HER and OER, respectively, with scan rate of 1 mV/s. The performance of overall water splitting was assessed in 1 M NaOH aqueous solution using a two-electrode configuration, and the LSV measurement was conducted at a scan rate of 1 mV/s. The longevity of CFeCoNiP-CFeCoNiP electrode-pair device for alkaline water electrolysis was evaluated using amperometry at a constant overpotential of 540 mV in 1 M NaOH electrolyte. All electrochemical measurements were performed at ambient temperature. All of the potentials were calibrated to a reversible hydrogen electrode (RHE) according to Nernst equation ($E_{RHE} = E_{SCE} + 0.05916pH + 0.244$; $E_{RHE} = E_{Hg/HgO} + 0.05916pH + 0.098$).[4] The equilibrium potential (E^{o}) for HER and OER is 0.00 V and 1.23 V vs RHE, respectively.

Electrochemical Capacitance Measurements. The electrochemically active surface area (ECSA), roughness factor (RF) and specific activity (j_s) of CFeP, CCoP, CNiP, CFeCoP, CFeNiP, CCoNiP and CFeCoNiP electrodes were estimated by electrochemical double-layer capacitance (C_{dl}) determined by cyclic voltammetry (CV) in 1 M NaOH aqueous solution.[5-6] The specific activity was measured at overpotentials of 100 and 350 mV for HER and OER, respectively. The potential range where there is a non-Faradaic current response was typically a 100 mV potential window centered on open-circuit potential (OCP) of the system. CV measurements were conducted in static solution by sweeping the potential across the non-Faradaic region from positive to negative potential and back at different scan rates. The working electrode was held at each potential vertex for 10 s before initiating the next sweep.

The electrochemically active surface area (ECSA) of a film-electrode sample is calculated from the measured double-layer capacitance (C_{dl}, mF) and specific capacitance (C_s, mF/cm^2).

$$ECSA = C_{dl} / C_s$$

Specific capacitance is the capacitance of an atomically smooth planar surface of the material per unit area under identical electrolyte condition. It has been reported that general specific capacitance is estimated as 0.04 mF/cm^2 in 1 M NaOH aqueous solution.[5-6] Roughness factor (RF) is then calculated by dividing ECSA by 0.08 cm^2, the geometric area of the electrode.

Electrical Impedance Spectroscopy (EIS). EIS measurements were carried out using a Zahner Zennium ε galvanostatic instrumentation with a standard three-electrode system. After LSV polarization curves were recorded, AC impedance measurements were conducted in the frequency range between 100 kHz and 100 mHz with AC modulation of 10 mV amplitude at overpotentials of 190 and 350 mV for HER and OER, respectively, in 1 M NaOH aqueous solution. Furthermore, in order to extract the true catalytic kinetics of an electrocatalyst, EIS measurements were performed consecutively at various overpotentials with interval as 5 mV. The applied overpotential for HER and OER is ranging from 1 to 30 mV and from 210 to 240 mV, respectively, for all electrocatalysts except that the overpotential range for CFeCoNiP cathode is 1 - 24 mV with interval of 4 mV owing to its high HER performance. The equivalent circuit was proposed to illustrate HER and OER impedance spectra.[7-9] The high frequency resistive response, R_e, represents the ohmic loss from electrolyte resistance. In this study, R_e value of 1 M NaOH electrolyte is in the range of 2.4 and 2.7 Ω. Film resistance (R_f) is related to the ohmic drop caused by the film resistivity and electrolyte resistance drop due to porous morphology of the film. Both polarization resistance (R_p) and surface intermediate resistance (R_s) are connected to the kinetics of the interfacial charge transfer reaction. When the applied potential during EIS measurement was relatively high, R_p and R_s are replaced with the combined charge transfer resistance (R_{ct}). In the whole cell, R_e is replaced by contact resistance (R_c) that describes ohmic loss derived from electrolyte resistance and the resistance between CFeCoNiP material and the support (Ni foam vs graphite plate). The complex nonlinear least-squares (CNLS) fitting of the impedance data was performed with Zview 3.0 software package. From the fitting results, only the logarithmic reciprocal of R_{ct} is plotted against the overpotential to obtain the corresponding kinetic Tafel slope, which could exactly reflect the inherent charge transfer kinetics of the catalyst material alone and exclude the influence of capacitive background, electrolyte resistance and film resistance.[9-11]

Determinations of Mass Activity and Faradaic Efficiency. The amounts of CFeCoNiP, CFeNiP,

CCoNiP, CCoP and CNiP catalysts cathodically deposited on the surface of graphite plate, determined by the weight differences of graphite plate before and after material deposition, is approximately 4.7, 3.2, 3.6, 3.5 and 3.2 mg/cm^2, respectively. Upon conducting OER in 1 M NaOH for 10 min, the amounts of CFeCoNiP, CFeNiP, CCoNiP, CCoP and CNiP catalysts on the surface of graphite plate were estimated as 4.5, 3.0, 3.4, 3.3 and 3.0 mg/cm^2, respectively. The value of mass activity (A/g) was calculated from the catalyst loading (m, mg/cm^2) and the measured current density (j, mA/cm^2) at overpotentials of 100 and 350 mV for HER and OER, respectively.

$$\text{mass activity} = j / m$$

A calibration curve was built by gas chromatography (SRI 8610C, molecular sieves (MS-13x) column and helium ionization detector (HID)) analysis via injection of the known amount of pure hydrogen and oxygen. The amount of hydrogen and oxygen dissolved in water was corrected by Henry's law (K_H = 7.8 × 10^{-4}mol/atm·L for H_2 and 1.3×10^{-3}mol/atm·L for O_2). The detection of hydrogen and oxygen was performed in two-compartment CV cell equipped with CFeCoNiP-CFeCoNiP electrode-pair setting in 1 M NaOH aqueous solution. Before the detection of the gas product, the cell is firmly sealed and subsequently purged with nitrogen for 30 min. Upon conducting the electrolysis at a current density of 100 mA/cm^2, the gas products were analyzed to determine Faradaic efficiency.

In Operando X-Ray Absorption Spectroscopy (XAS). All metal XAS K edge spectra were carried out at NSRRC, Hsinchu, Taiwan and were recorded at ambient temperature. Experiments were performed in transmission mode at TPS 44A beamline with a double crystal Si(111) monochromator. The energy resolution ΔE/E was estimated to be about 2 × 10^{-4}. High harmonics were rejected by Rh-coated mirrors. The Fe, Co and Ni Kedge spectra were scanned from 6.912 to 7.609 keV, from 7.509 to 8.233 keV and from 8.133 to 9.240 keV, respectively. The reference Fe, Co and Ni foils were always measured simultaneously, in which the first inflection point at 7112.0 eV (Fe), 7709.0 eV (Co) and 8333.0 eV (Ni) in XAS spectra were used for energy calibration. Ion chambers used to measure the incident (I_0) and transmitted (I_t) beam intensities were filled with a mixture of N_2 and He gases and a mixture of N_2 and Ar gases, respectively.

For in operando metal K edge XAS experiments, carbon fiber paper was applied as working electrode. The amperometric method with applied potential at -1.0 V was used to deposit FeCoNi-based electrocatalyst on the surface of carbon fiber paper, and the deposition time was around 3 h (film thickness 168.3 μm) or

100 s (film thickness 389.2 nm). Also, an in operando setup (Figure S25) was applied using Kapton films to cover the central hole which serves as the window for incident X-ray beam. The catalyst-loaded carbon fiber paper is carefully pushed toward the inner part of Kapton film, and the thickness of 1 M NaOH aqueous electrolyte between catalyst and Kapton film is estimated to be less than 500 μm. During the measurements, the catalyst was polarized at a desired potential and was held until a stable current obtained. After that, this applied potential was held for additional 10 min to finish Fe/Co/Ni K edge XAS measurements (0.5 s per scan) before applying the next desired potentials. The step size of in operando XAS measurements at Fe, Co and Ni K edge was 0.35, 0.38 and 0.41 eV, respectively. The acquired XANES and EXAFS data were processed to be normalized to the edge jump as 1.0 using Athena module implemented in the IFEFFIT software packages. The k weight in the background function determination was set to 2, and the frequency cut off parameter, Rb kg, was set to 1. The k^3-weighted $\chi(k)$ data of Fe/Co/Ni K edges were Fourier transformed to real R space using the hanning window function (Δk = 1 $Å^{-1}$) to separate EXAFS contributions from different coordination shells. The Artemis code was used to obtain the quantitative structural parameters by least-squares fitting. The detailed fitting information on Fe/Co/Ni EXAFS data was described in Figures S17-S20 and summarized in Tables S6 and S7.

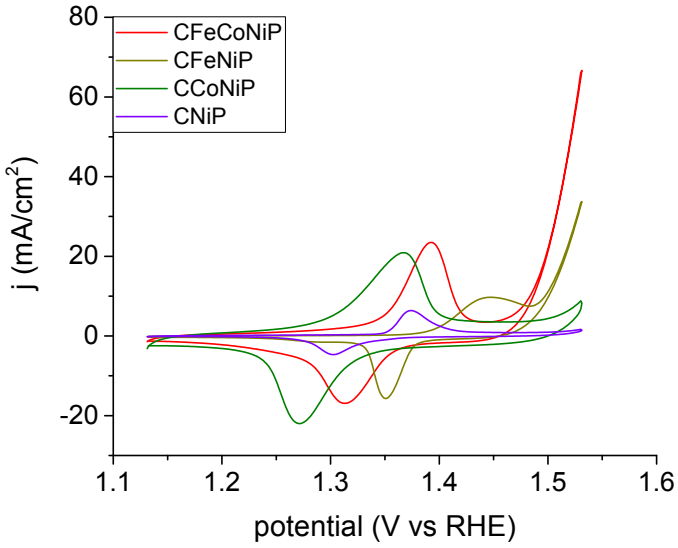

Figure S1. CV data (50 mV/s) showing Ni^{2+}/Ni^{3+} redox features of Ni-containing electrocatalysts in 1 M NaOH aqueous electrolyte.

(a)

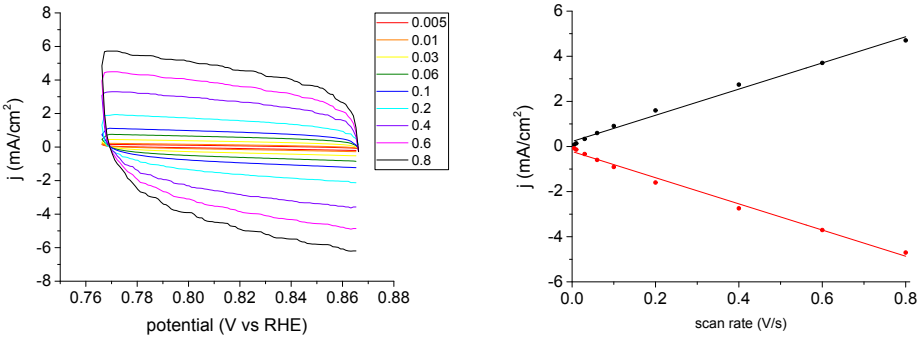

(b)

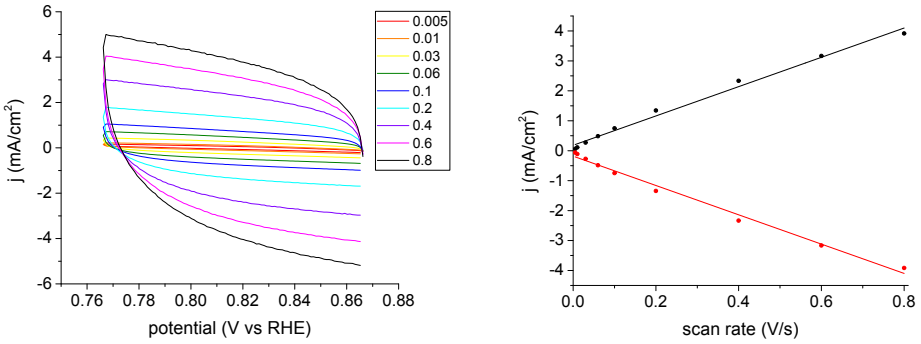

(c)

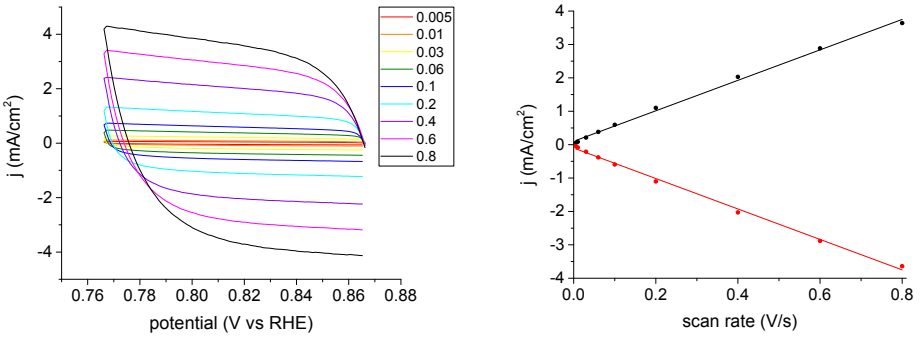

(d)

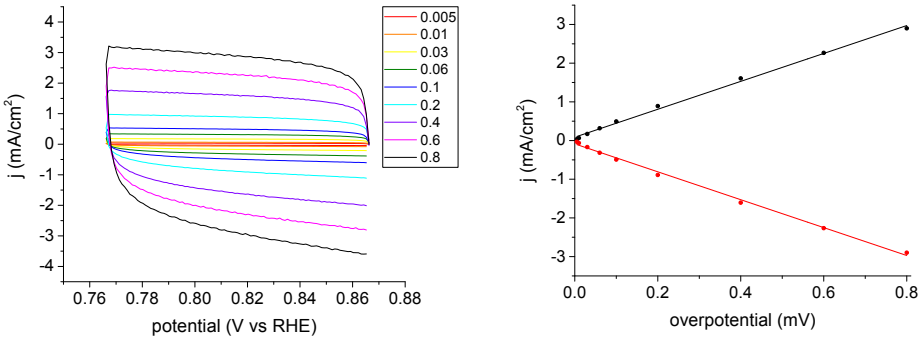

Figure S2. Double-layer capacitance (C_{dl}) measured in 1 M NaOH aqueous solution to determine roughness factor (RF) for HER. (a) CFeCoNiP electrode (C_{dl} = 5.81 mF/cm^2, RF = 145.1), (b) CFeNiP electrode (C_{dl} = 4.89 mF/cm^2, RF = 122.3), (c) CCoNiP electrode (C_{dl} = 4.58 mF/cm^2, RF = 114.3), and (d) CNiP electrode (C_{dl} = 3.61 mF/cm^2, RF = 90.2).

(a)

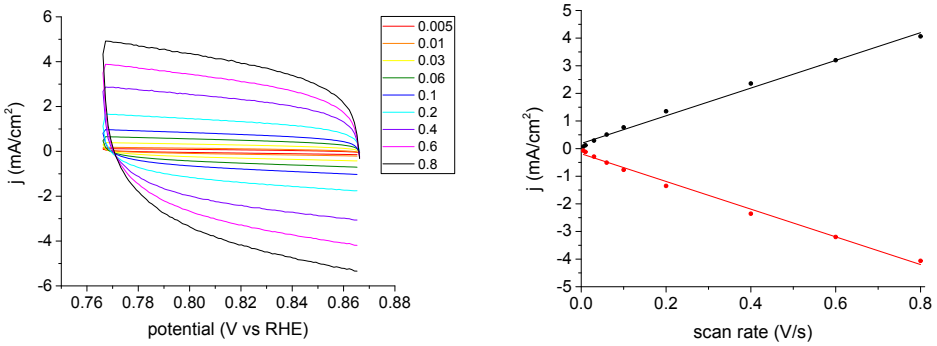

(b)

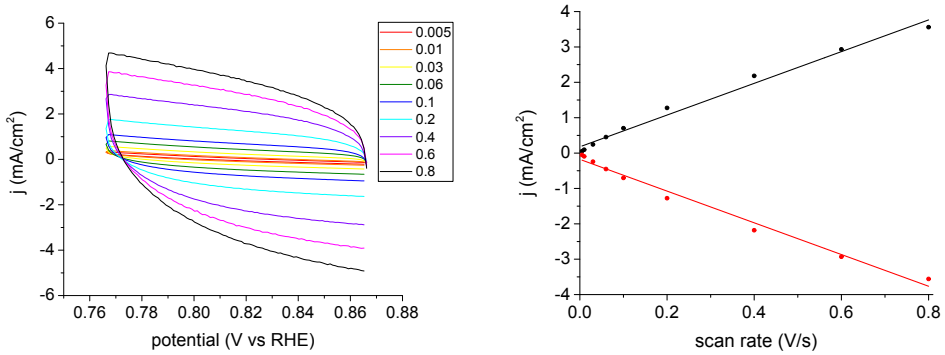

(c)

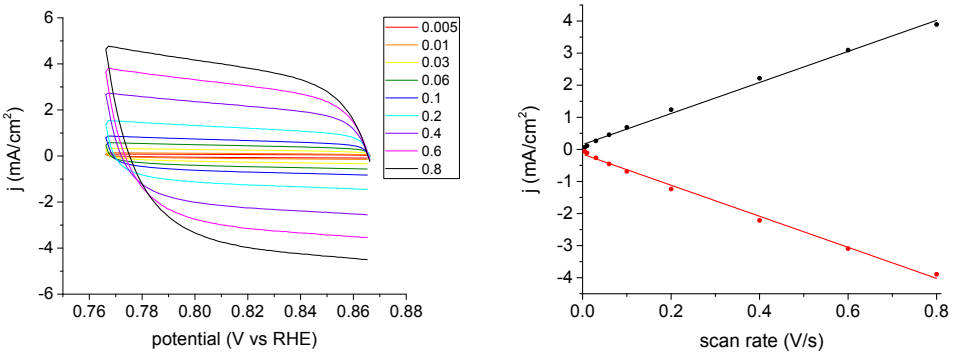

(d)

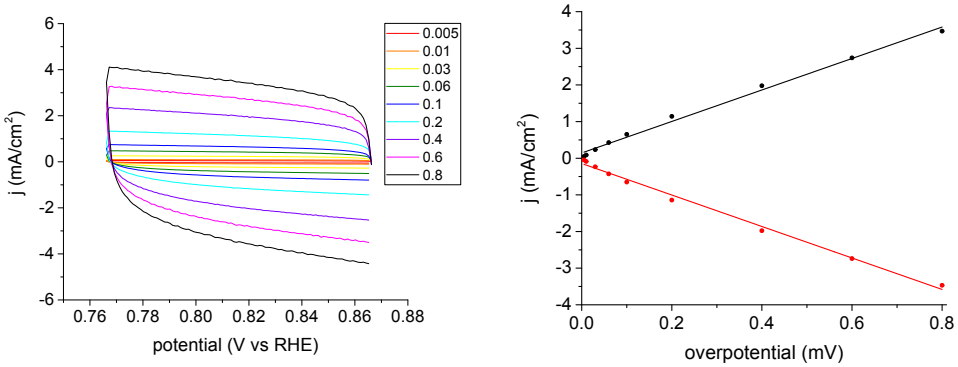

Figure S3. Double-layer capacitance (C_{dl}) measured in 1 M NaOH aqueous solution to determine roughness factor (RF) for OER. (a) CFeCoNiP electrode (C_{dl} = 5.02 mF/cm^2, RF = 125.4), (b) CFeNiP electrode (C_{dl} = 4.49 mF/cm^2, RF = 112.1), (c) CCoNiP electrode (C_{dl} = 4.85 mF/cm^2, RF = 121.0), and (d) CNiP electrode (C_{dl}= 4.30 mF/cm^2, RF = 107.4).

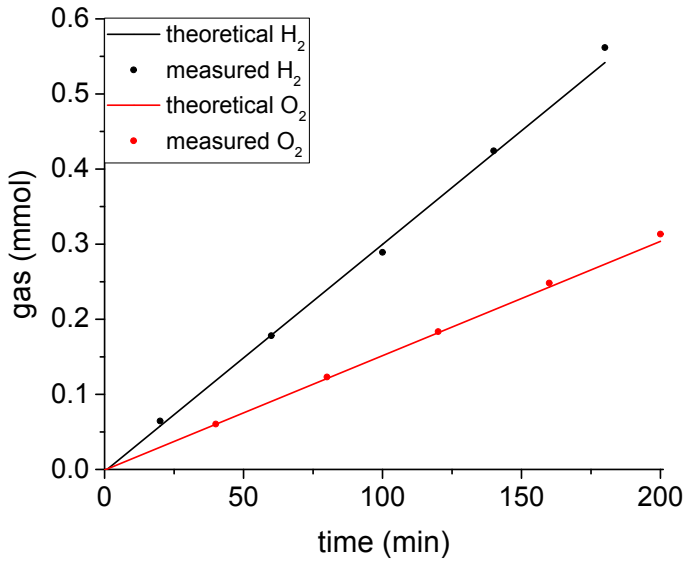

Figure S4. The amount of H_2 and O_2 gases obtained by theoretical calculation and experimental measurements versus time for electrolysis with current density of 100 mA/cm^2 in 1 M NaOH aqueous solution by using CFeCoNiP-CFeCoNiP electrode-pair setting (η = 540 mV).

(a)

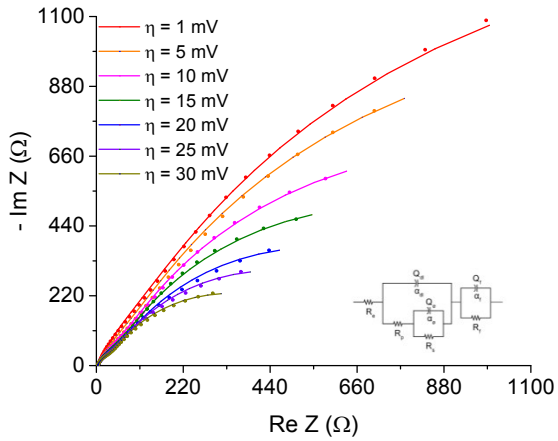
η = 1 mV
η = 5 mV
η = 10 mV
η = 15 mV
η = 20 mV
η = 25 mV
η = 30 mV
- Im Z (Ω)
Re Z (Ω)
0
220
440
660
880
1100

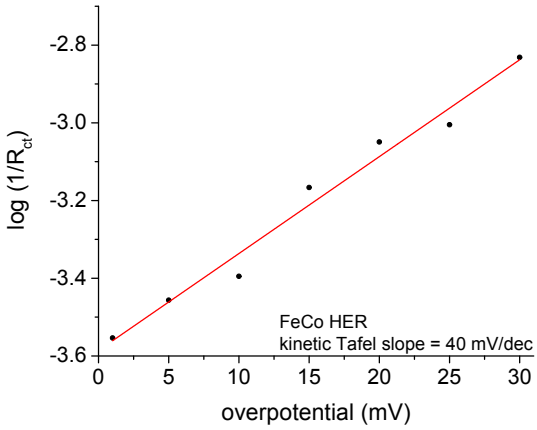
log (1/R_ct)
overpotential (mV)
FeCo HER
kinetic Tafel slope = 40 mV/dec
-2.8
-3.0
-3.2
-3.4
-3.6
0
5
10
15
20
25
30

(b)

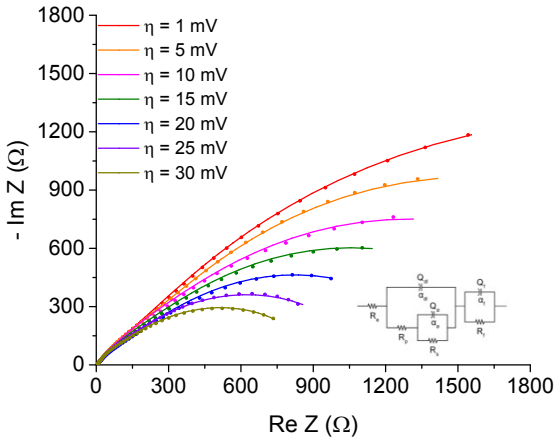
η = 1 mV
η = 5 mV
η = 10 mV
η = 15 mV
η = 20 mV
η = 25 mV
η = 30 mV
- Im Z (Ω)
Re Z (Ω)
0
300
600
900
1200
1500
1800

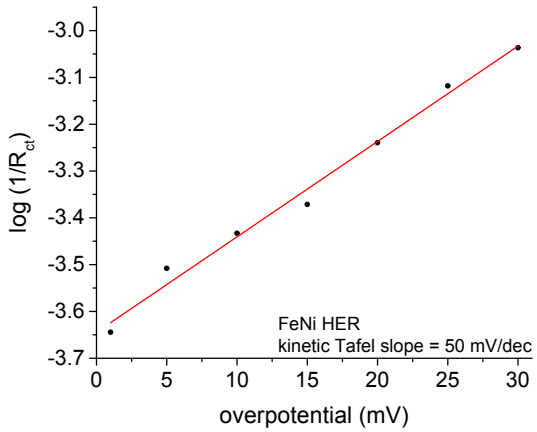
log (1/R_ct)
overpotential (mV)
FeNi HER
kinetic Tafel slope = 50 mV/dec
-3.0
-3.1
-3.2
-3.3
-3.4
-3.5
-3.6
-3.7
0
5
10
15
20
25
30

(c)

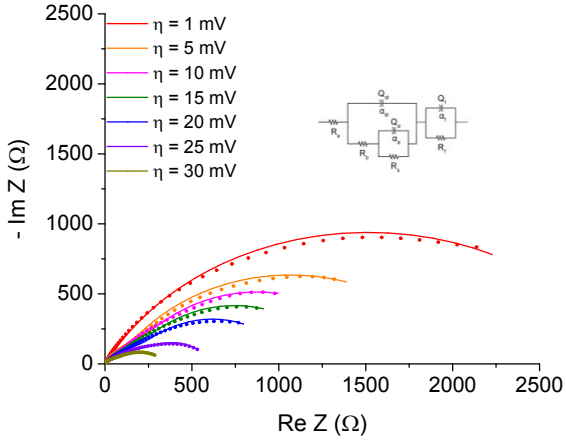
η = 1 mV
η = 5 mV
η = 10 mV
η = 15 mV
η = 20 mV
η = 25 mV
η = 30 mV
- Im Z (Ω)
Re Z (Ω)
0
500
1000
1500
2000
2500

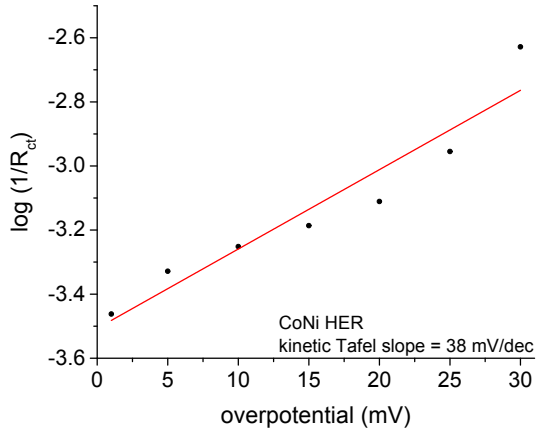
log (1/R_ct)
overpotential (mV)
CoNi HER
kinetic Tafel slope = 38 mV/dec
-2.6
-2.8
-3.0
-3.2
-3.4
-3.6
0
5
10
15
20
25
30

(d)

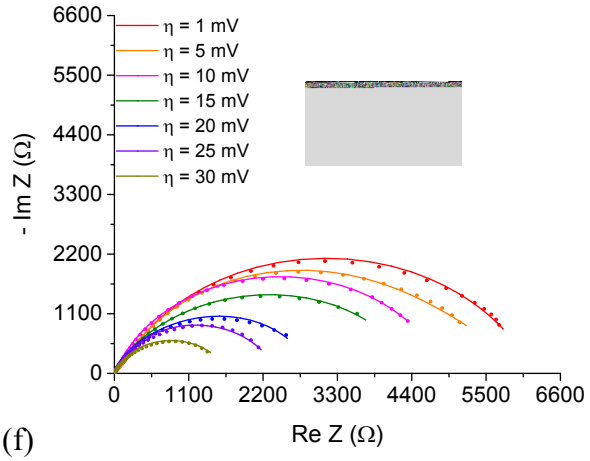

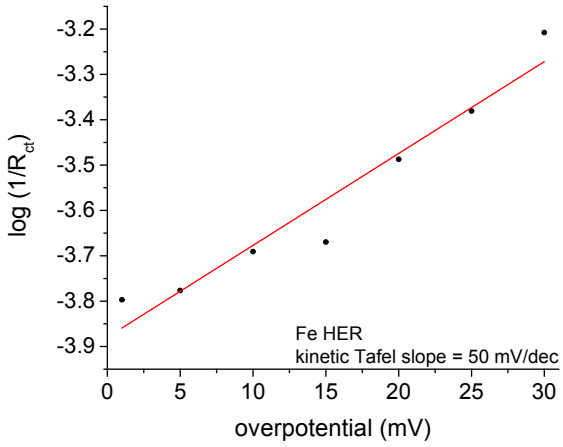

(f)

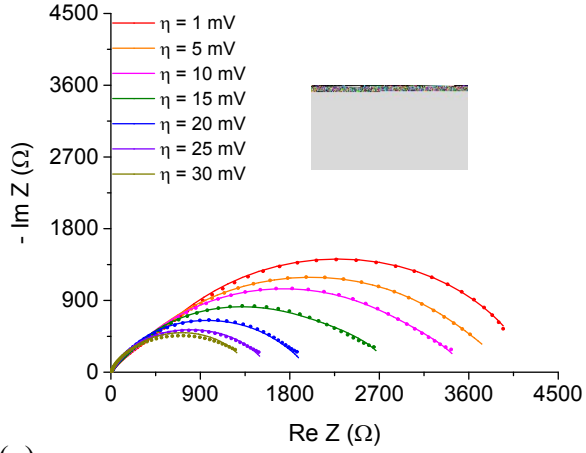

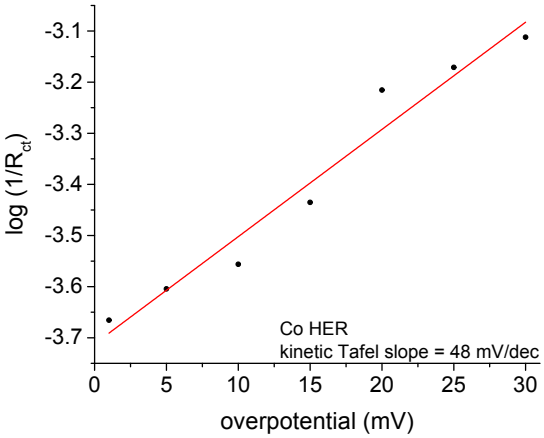

(g)

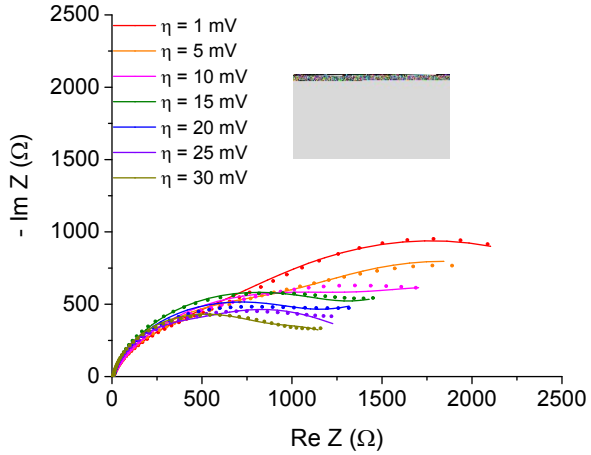

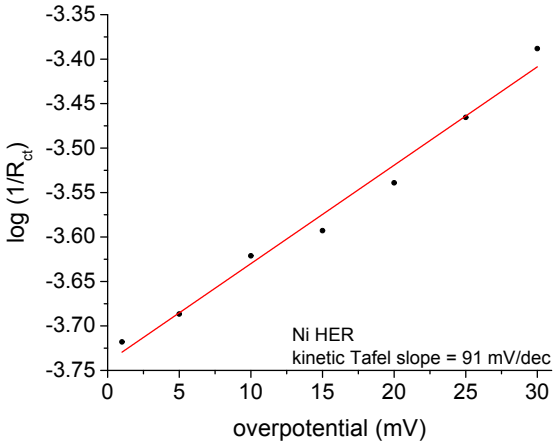

Figure S5. The Nyquist plots and kinetric Tafel slope derived from the plots of log ($1/R_{ct}$) vs overpotential for (a) CFeCoP, (b) CFeNiP, (c) CCoNiP, (d) CFeP, (e) CCoP, and (f) CNiP cathodes in 1 M NaOH aqueous electrolyte.

(a)

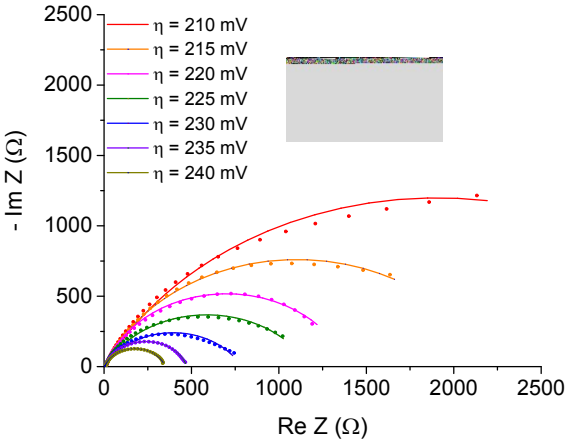
η = 210 mV
η = 215 mV
η = 220 mV
η = 225 mV
η = 230 mV
η = 235 mV
η = 240 mV
- Im Z (Ω)
Re Z (Ω)
0
500
1000
1500
2000
2500

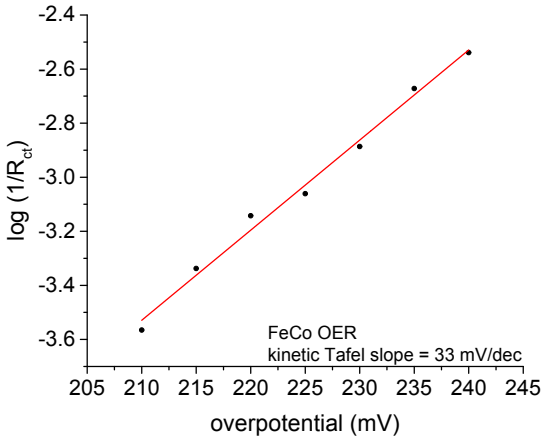
log (1/R_ct)
overpotential (mV)
FeCo OER
kinetic Tafel slope = 33 mV/dec
-2.4
-2.6
-2.8
-3.0
-3.2
-3.4
-3.6
205
210
215
220
225
230
235
240
245

(b)

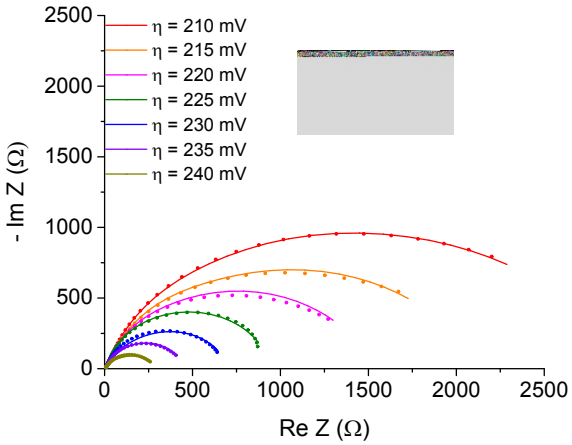
η = 210 mV
η = 215 mV
η = 220 mV
η = 225 mV
η = 230 mV
η = 235 mV
η = 240 mV
- Im Z (Ω)
Re Z (Ω)
0
500
1000
1500
2000
2500

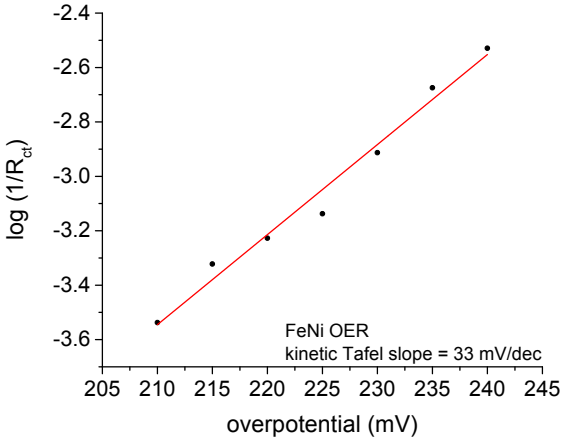
log (1/R_ct)
overpotential (mV)
FeNi OER
kinetic Tafel slope = 33 mV/dec
-2.4
-2.6
-2.8
-3.0
-3.2
-3.4
-3.6
205
210
215
220
225
230
235
240
245

(c)

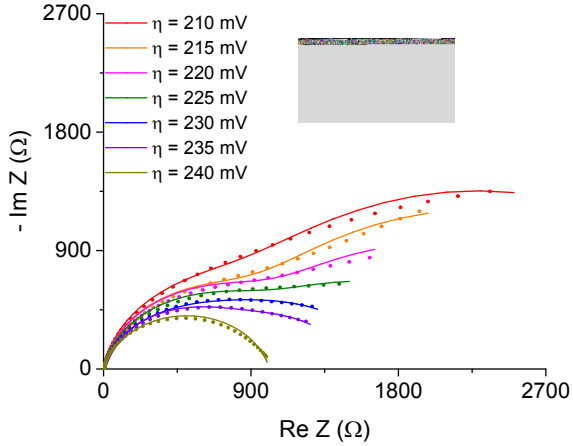
η = 210 mV
η = 215 mV
η = 220 mV
η = 225 mV
η = 230 mV
η = 235 mV
η = 240 mV
- Im Z (Ω)
Re Z (Ω)
0
900
1800
2700

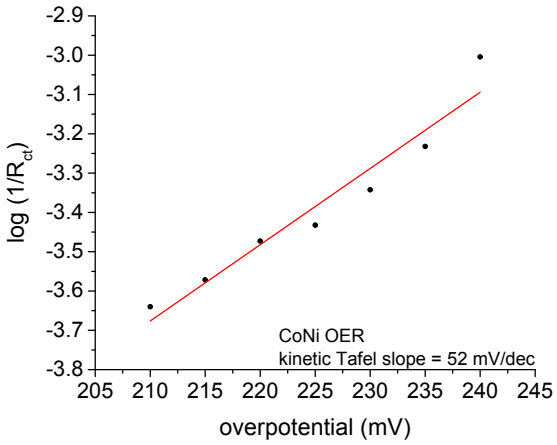
log (1/R_ct)
overpotential (mV)
CoNi OER
kinetic Tafel slope = 52 mV/dec
-2.9
-3.0
-3.1
-3.2
-3.3
-3.4
-3.5
-3.6
-3.7
-3.8
205
210
215
220
225
230
235
240
245

(d)

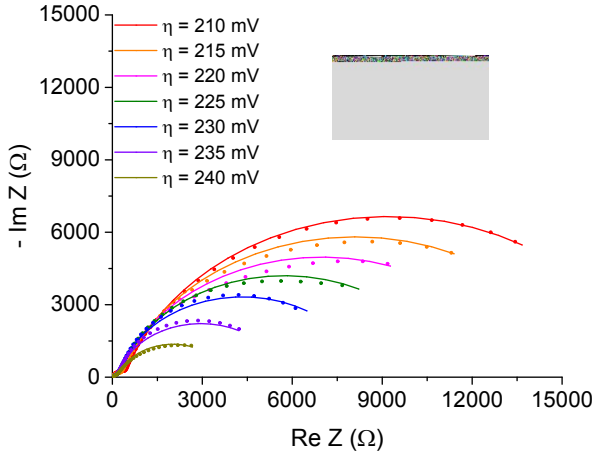

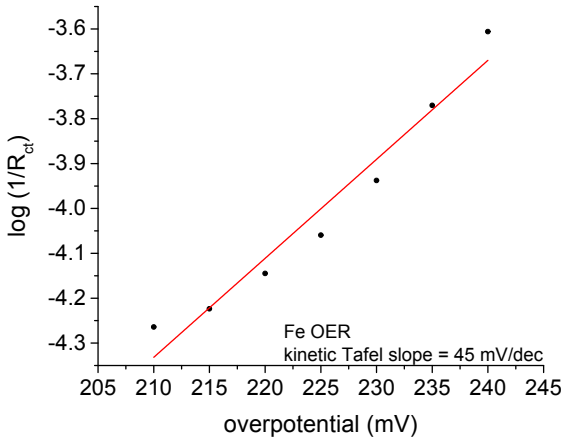

(e)

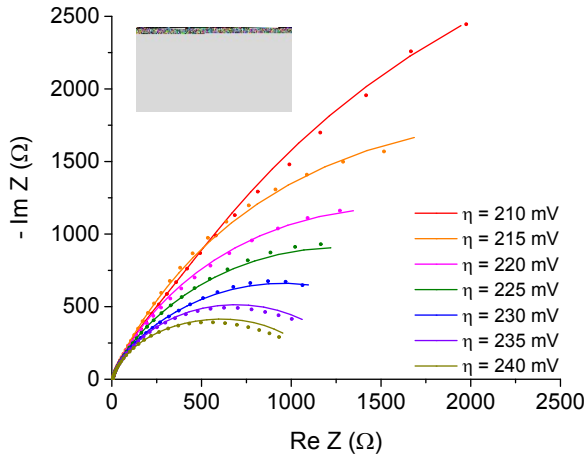

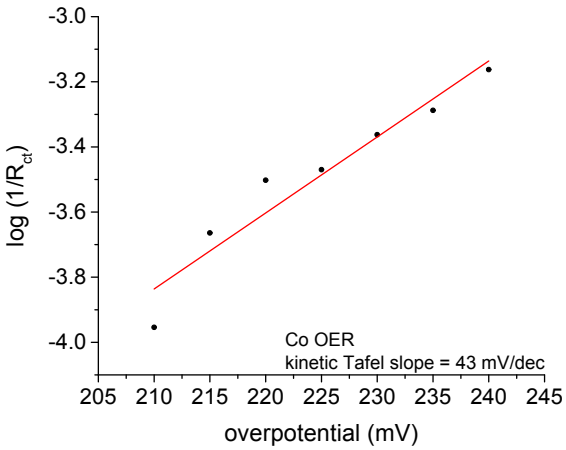

(f)

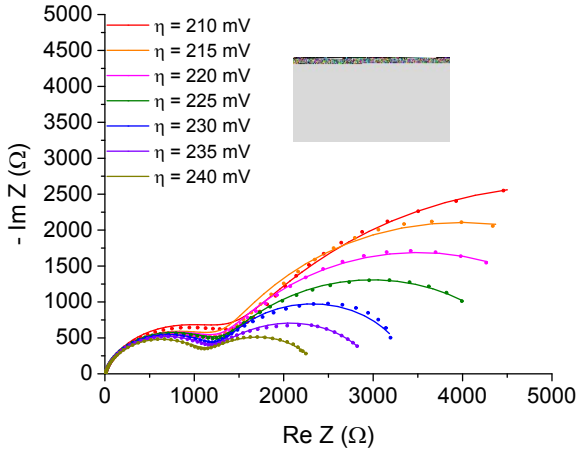

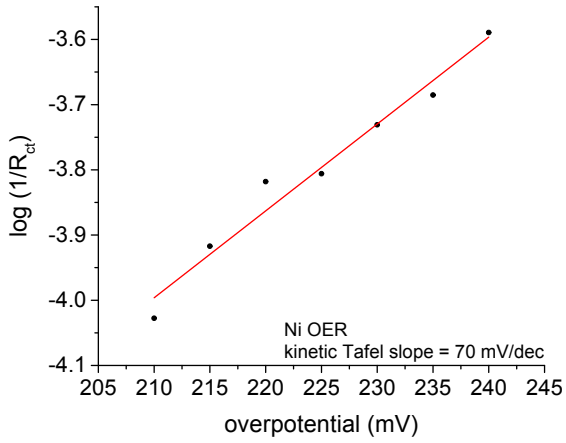

Figure S6. The Nyquist plots and kinetric Tafel slope derived from the plots of log ($1/R_{ct}$) vs overpotential for (a) CFeCoP, (b) CFeNiP, (c) CCoNiP, (d) CFeP, (e) CCoP, and (f) CNiP anodes in 1 M NaOH aqueous electrolyte.

(a)

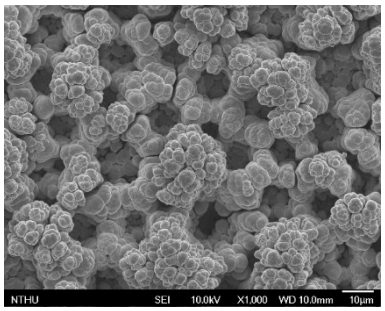

(b)

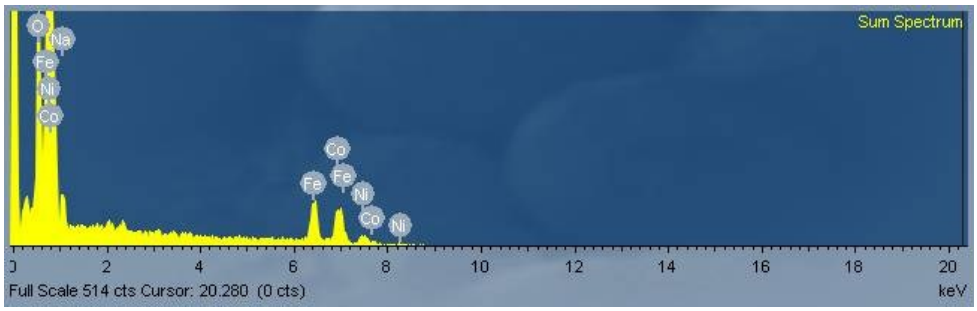

(c)

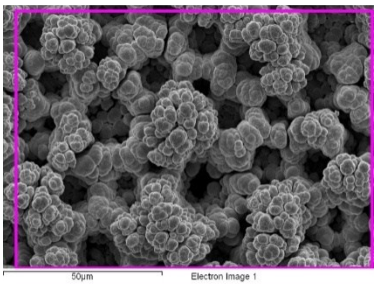

(d)

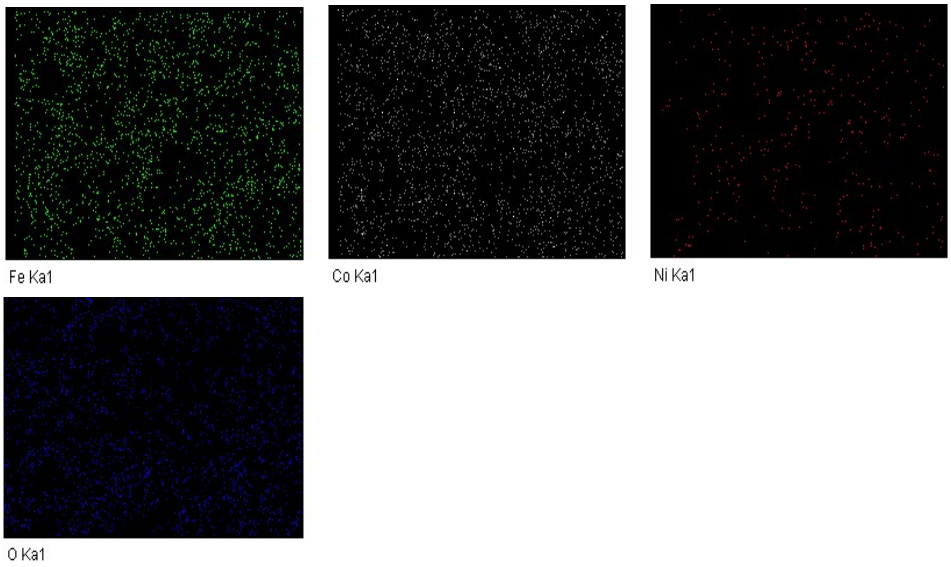

(e)

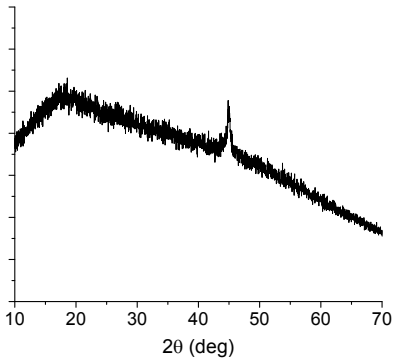

Figure S7. (a) SEM image, (b) EDX spectrum, (c)-(d) SEM-EDX elemental maps (Fe, Co, Ni and O elements are shown as green, white, red and blue), and (e) pXRD pattern of CFeCoNiP cathode.

(a) (b)

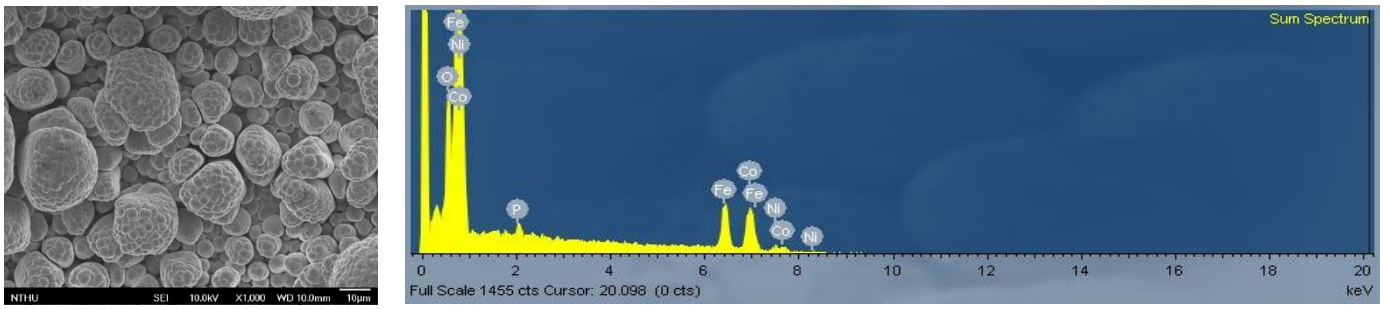

(c) (d)

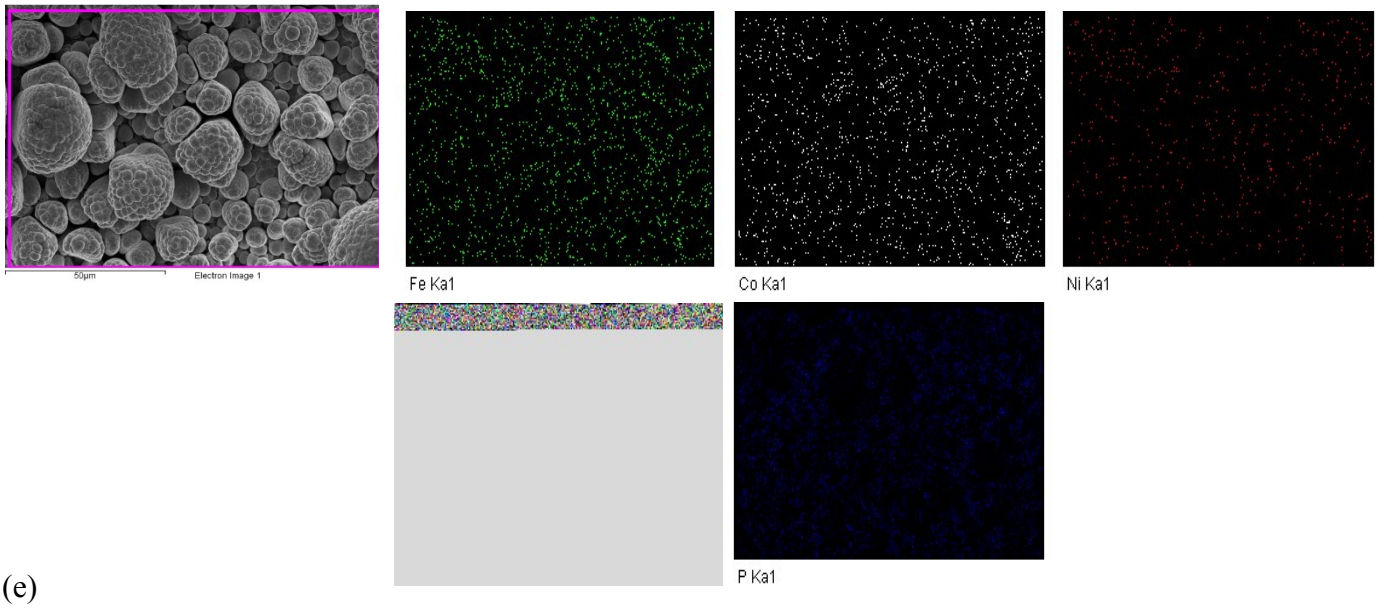

(e)

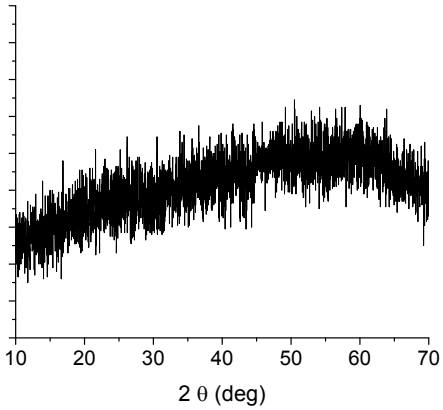

Figure S8. (a) SEM image, (b) EDX spectrum, (c)-(d) SEM-EDX elemental maps (Fe, Co, Ni, O and P elements are shown as green, white, red, blue and blue), and (e) pXRD pattern of CFeCoNiP anode.

(a)

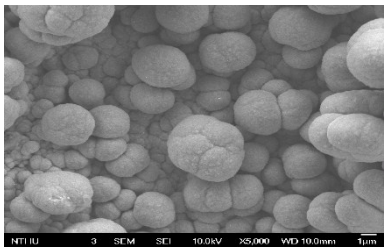

(b)

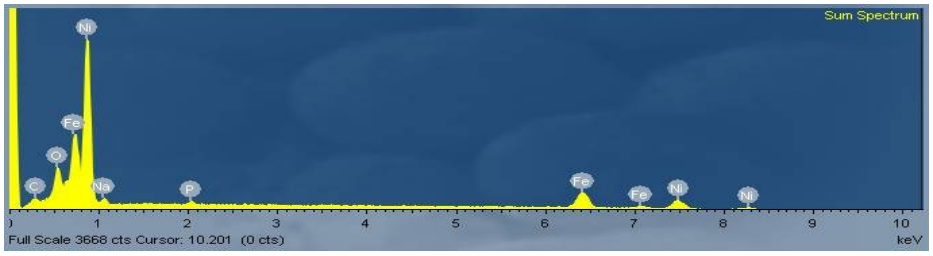

(c)

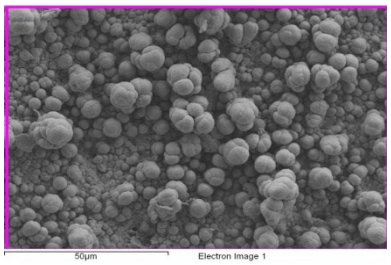

(d)

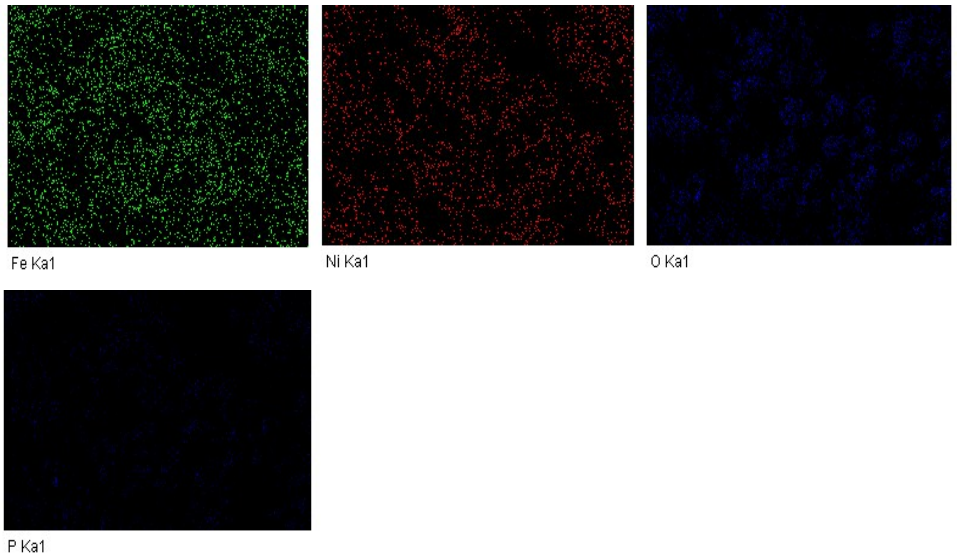

Figure S9. (a) SEM image, (b) EDX spectrum, (c)-(d) SEM-EDX elemental maps (Fe, Ni, O and P elements are shown as green, red, blue and blue) of CFeNiP cathode.

(a) (b)

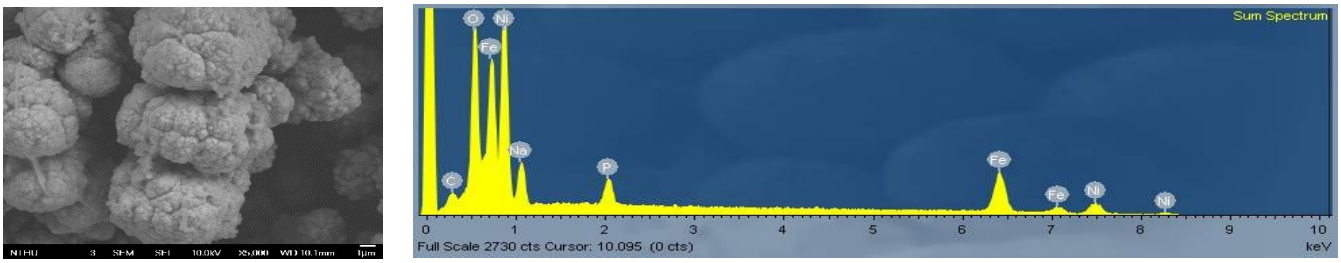

(c) (d)

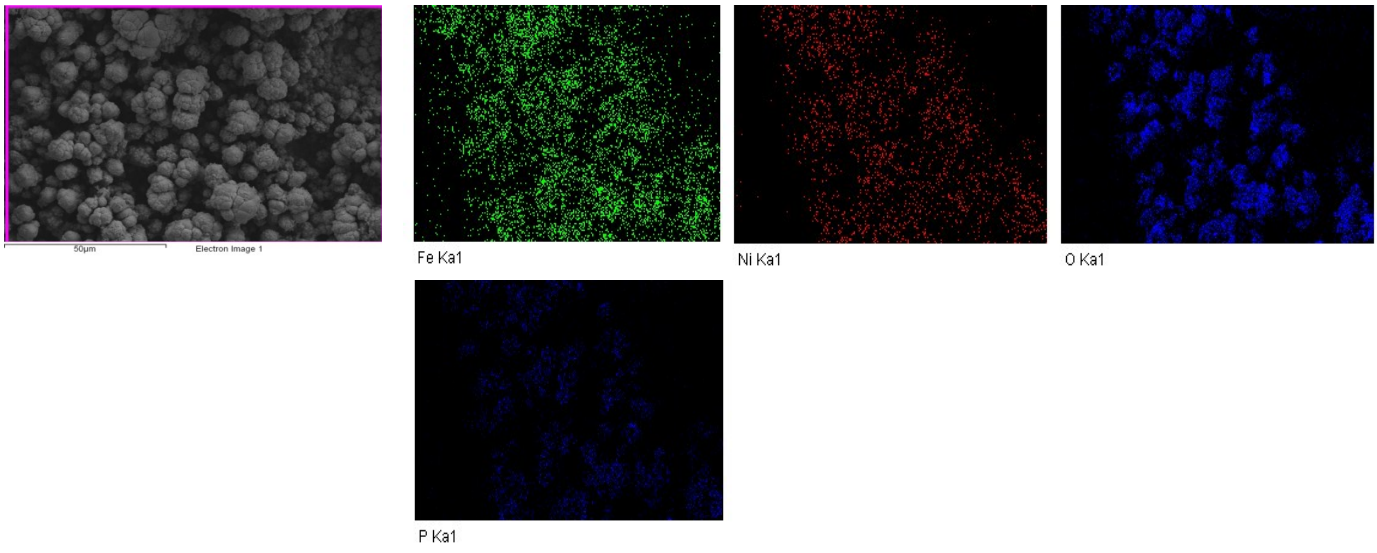

Figure S10. (a) SEM image, (b) EDX spectrum, (c)-(d) SEM-EDX elemental maps (Fe, Ni, O and P elements are shown as green, red, blue and blue) of CFeNiP anode.

(a) (b)

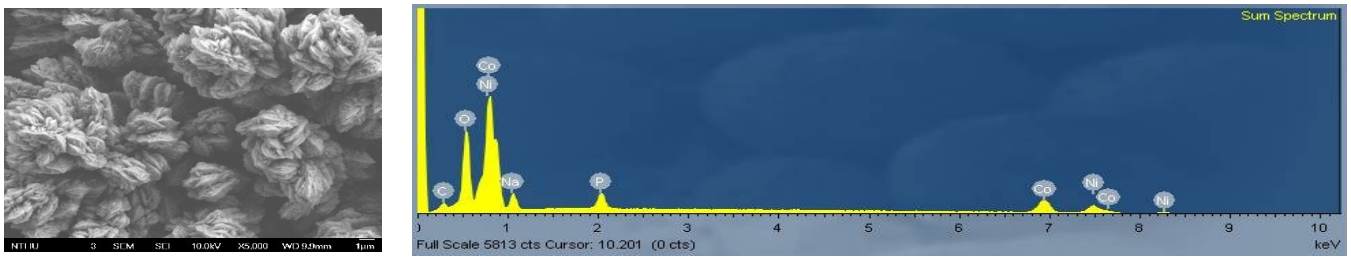

(c) (d)

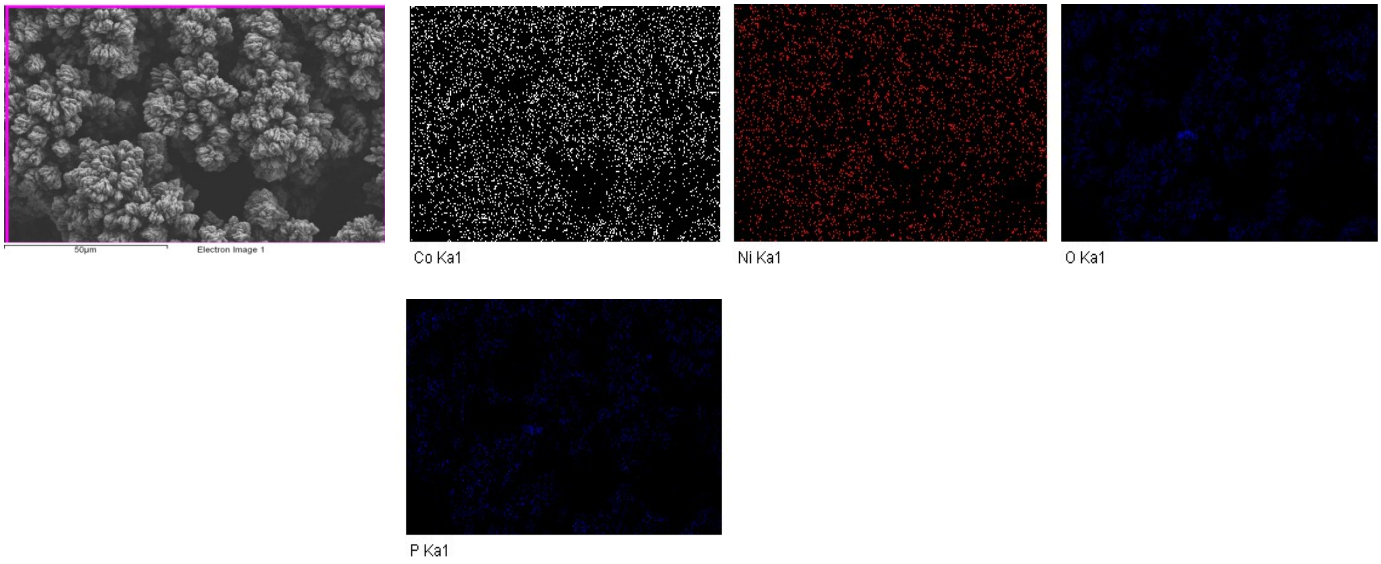

Figure S11. (a) SEM image, (b) EDX spectrum, (c)-(d) SEM-EDX elemental maps (Co, Ni, O and P elements are shown as white, red, blue and blue) of CCoNiP cathode.

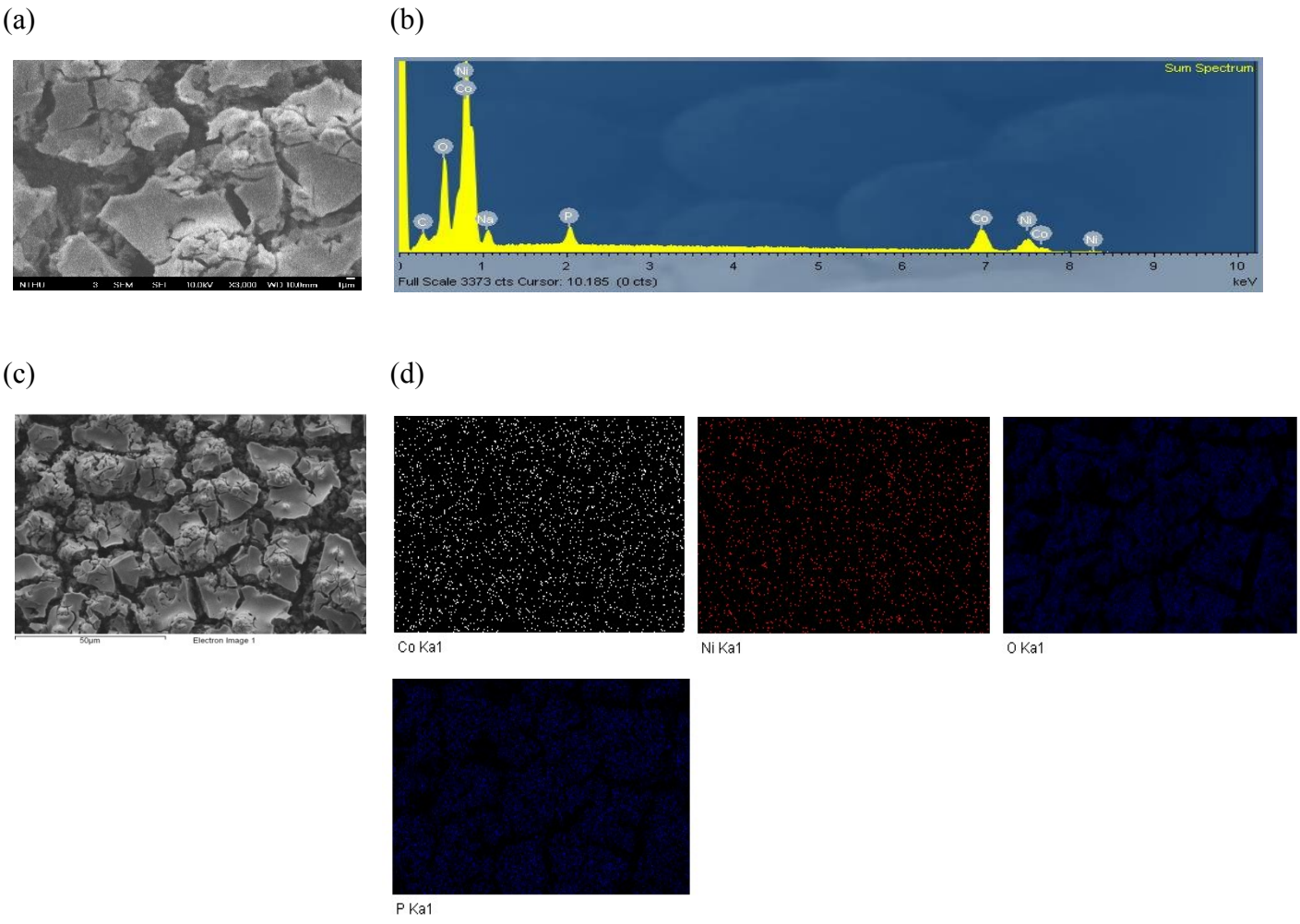

Figure S12. (a) SEM image, (b) EDX spectrum, (c)-(d) SEM-EDX elemental maps (Co, Ni, O and P elements are shown as white, red, blue and blue) of CCoNiP anode.

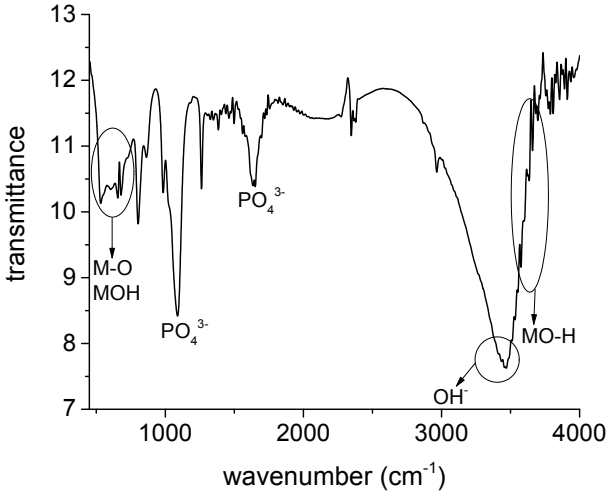

Figure S13. FT-IR spectrum of CFeCoNiP electrode. M is denoted as Fe, Co and Ni.

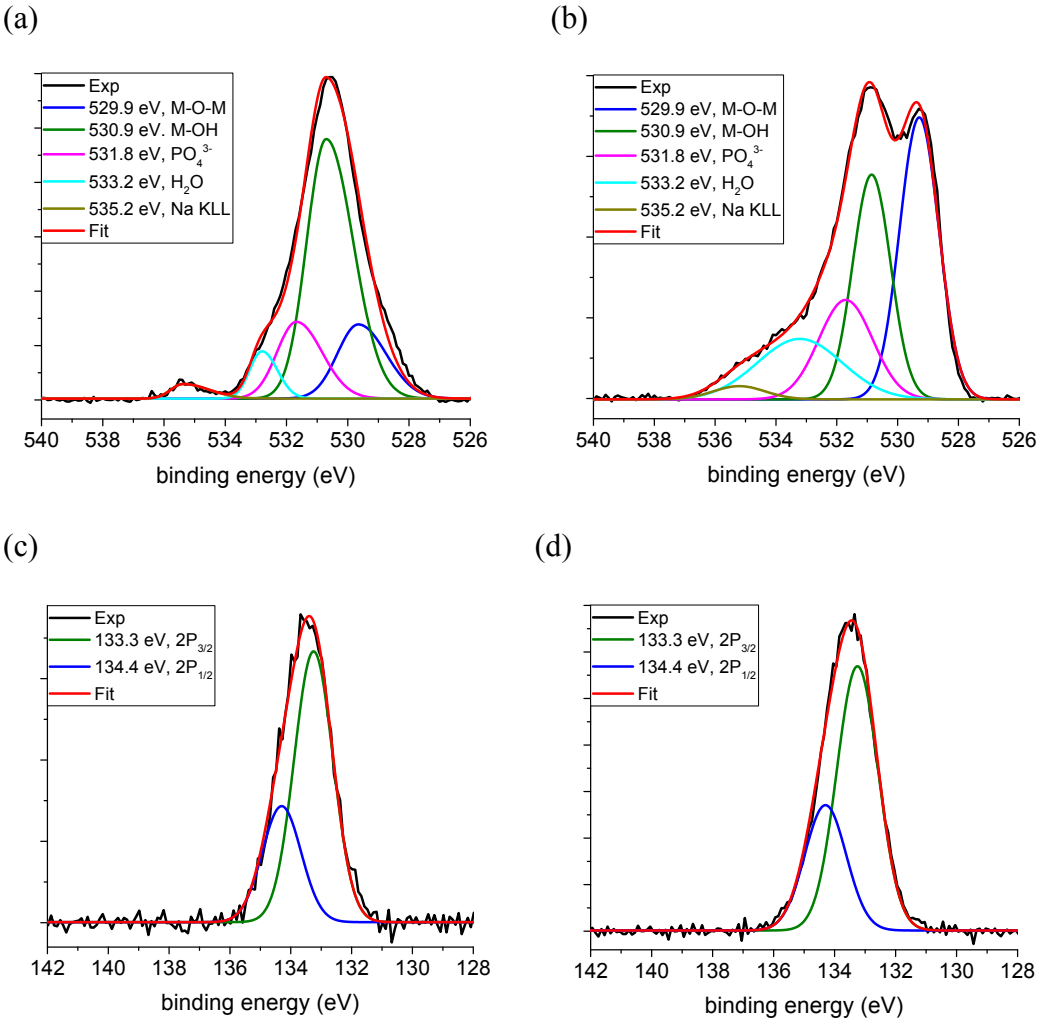

Figure S14. XPS spectra of CFeCoNiP electrode. (a) O1s of cathode, (b) O 1s of anode, and (c) P 2p of cathode, (e) P 2p of anode. M is denoted as metal, Fe, Co and Ni.

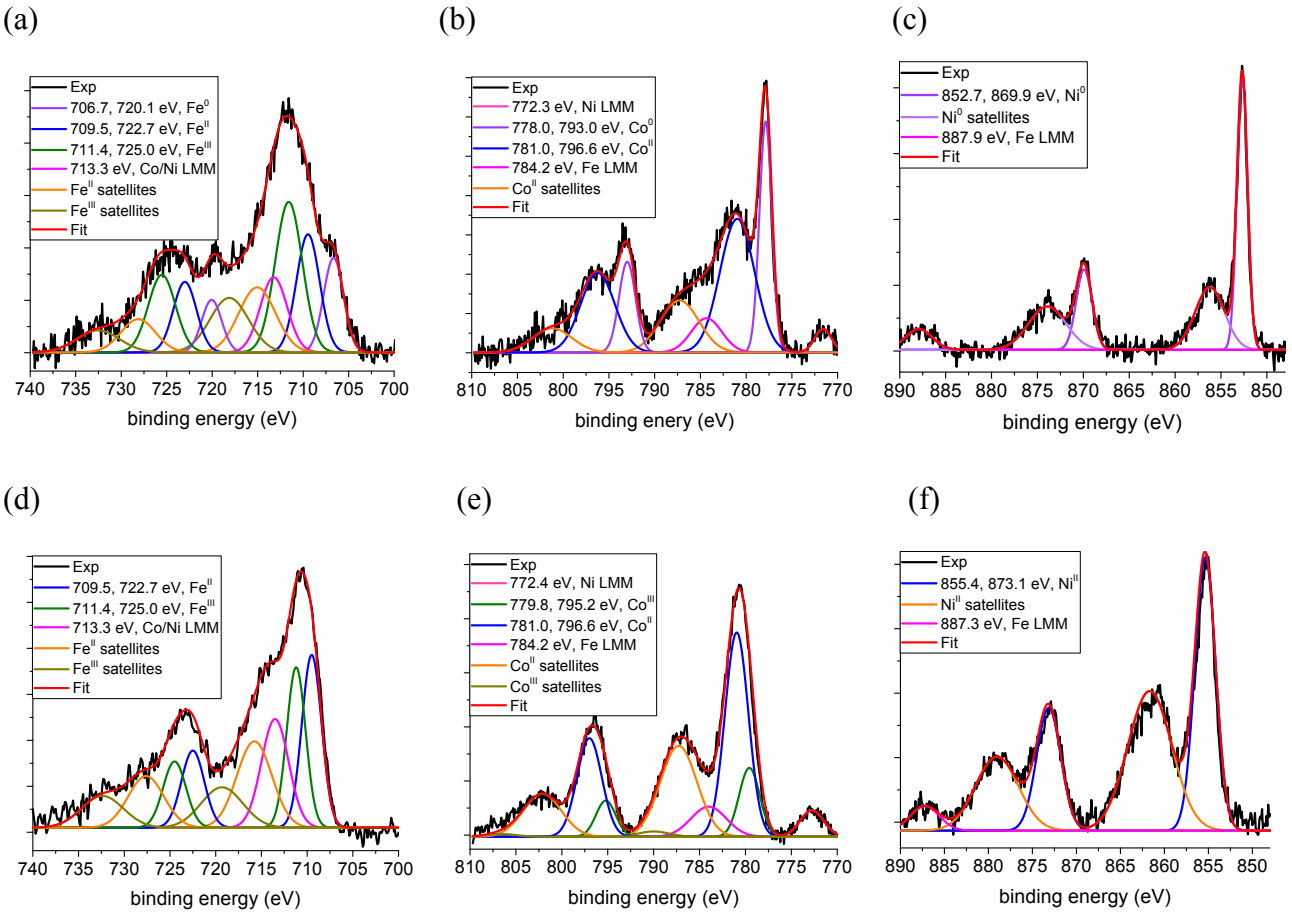

Figure S15. XPS spectra of CFeCoNiP electrode. (a) Fe 2p of cathode, (b) Co 2p of cathode, (c) Ni 2p of cathode, and (d) Fe 2p of anode, (e) Co 2p of anode, (f) Ni 2p anode.

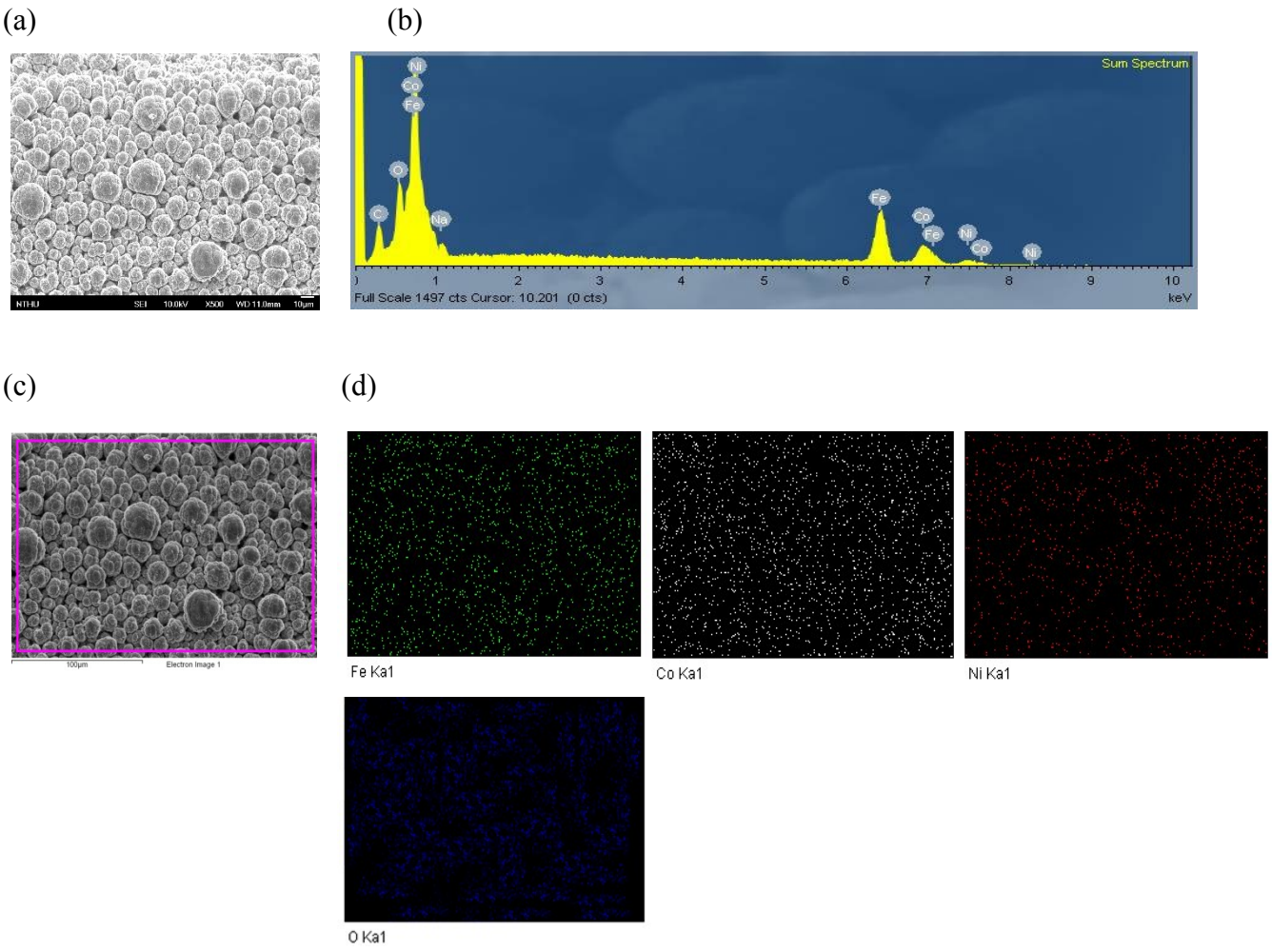

Figure S16. (a) SEM image, (b) EDX spectrum, (c)-(d) SEM-EDX elemental maps (Fe, Co, Ni and O elements are shown as green, white, red and blue) of CFeCoNiP cathode after alkaline water splitting for 139 h.

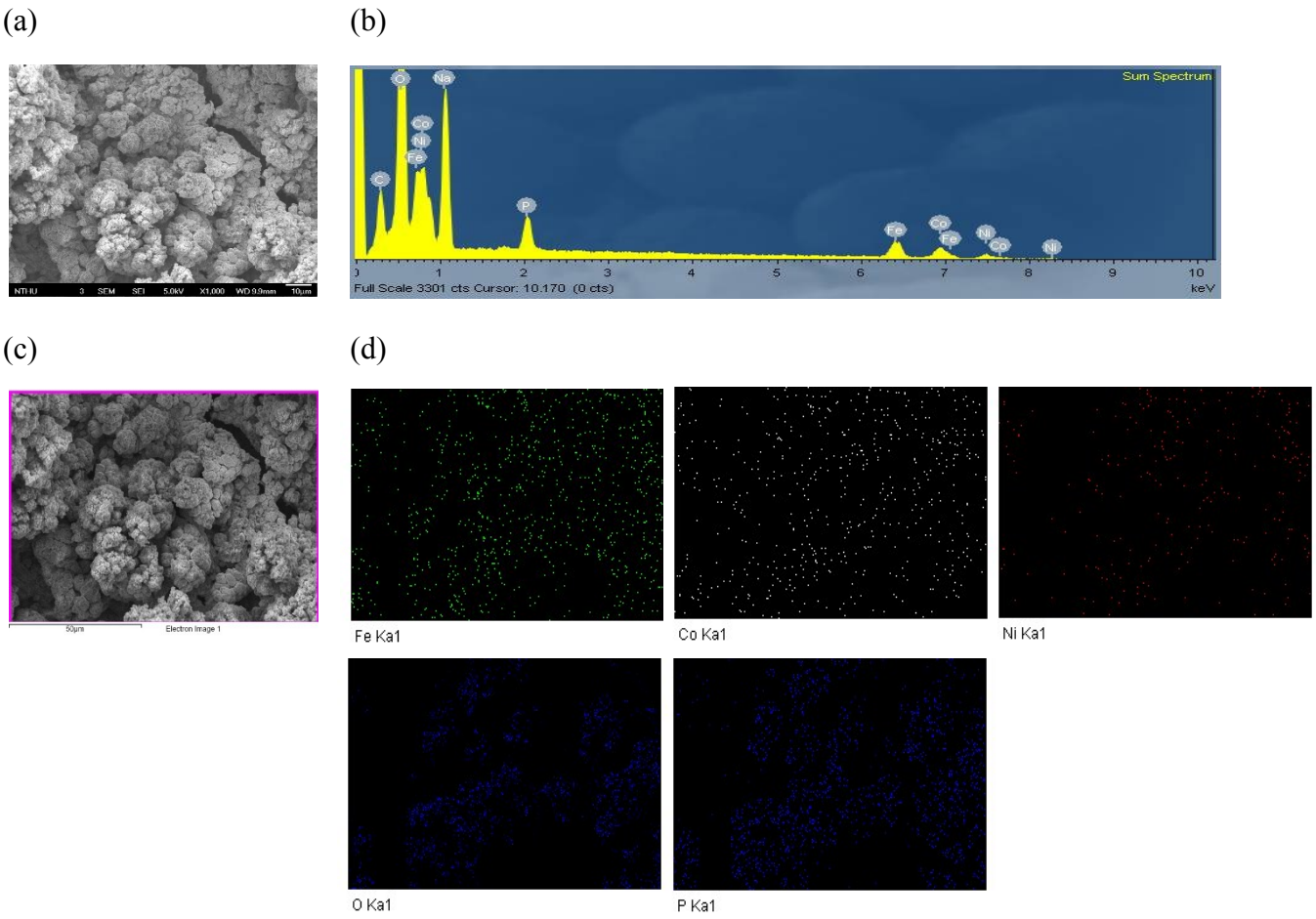

Figure S17. (a) SEM image, (b) EDX spectrum, (c)-(d) SEM-EDX elemental maps (Fe, Co, Ni, O and P elements are shown as green, white, red, blue and blue) of CFeCoNiP anode after alkaline water splitting for 139 h.

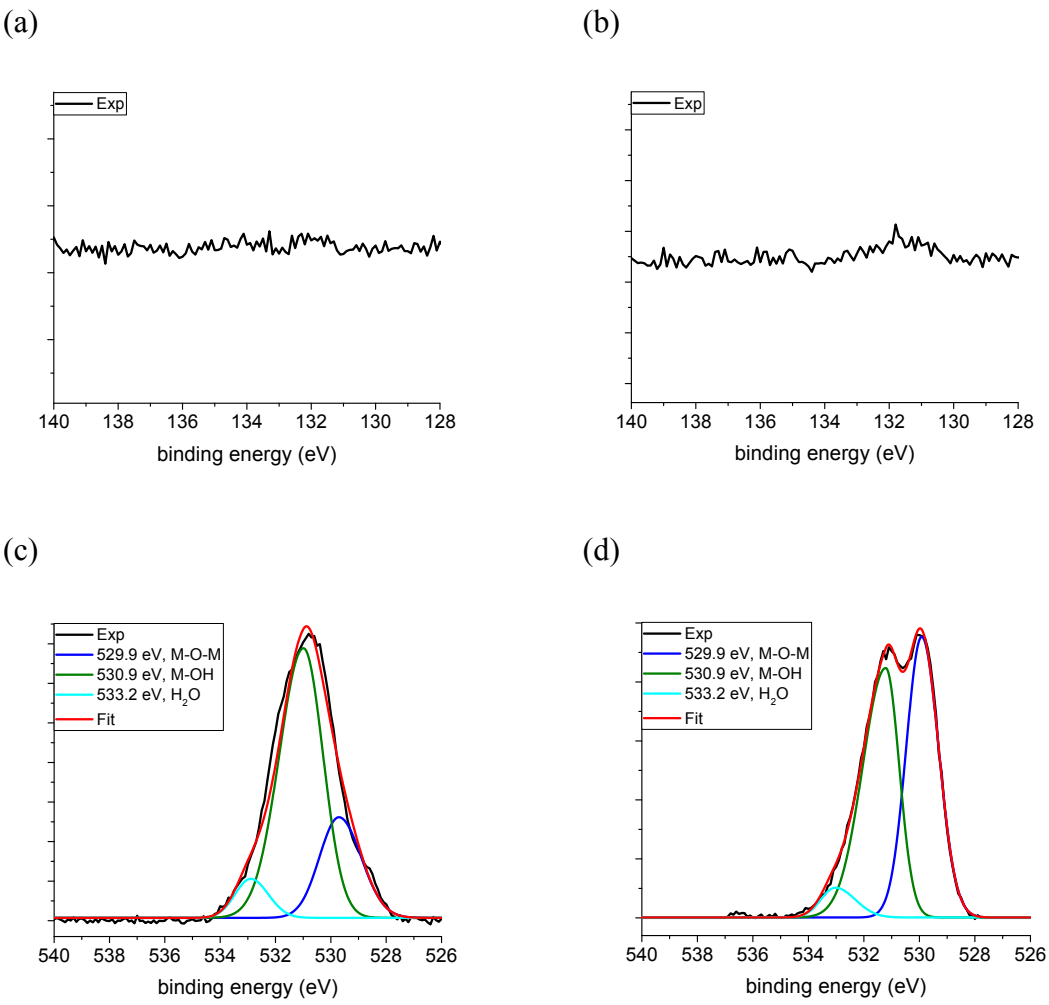

Figure S18. XPS spectra of CFeCoNiP electrode-pair setting after alkaline water splitting for 139 h. (a) P 2p of cathode, (b) P 2p of anode, and (c) O 1s of cathode, (d) O 1s of anode.

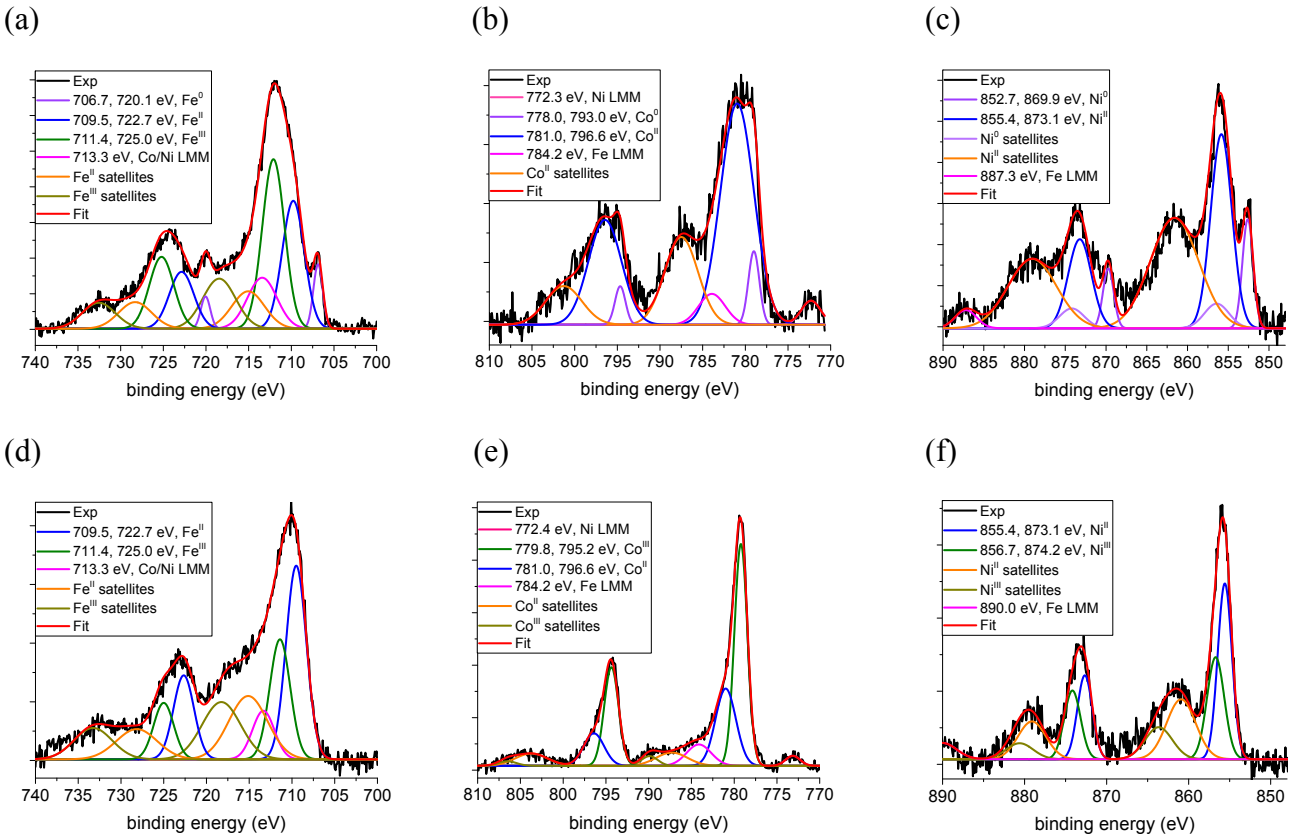

Figure S19. XPS spectra of CFeCoNiP electrode-pair setting after alkaline water splitting for 139 h. (a) Fe 2p of cathode, (b) Co 2p of cathode, (c) Ni 2p of cathode, and (d) Fe 2p of anode, (e) Co 2p of anode, (f) Ni 2p of anode.

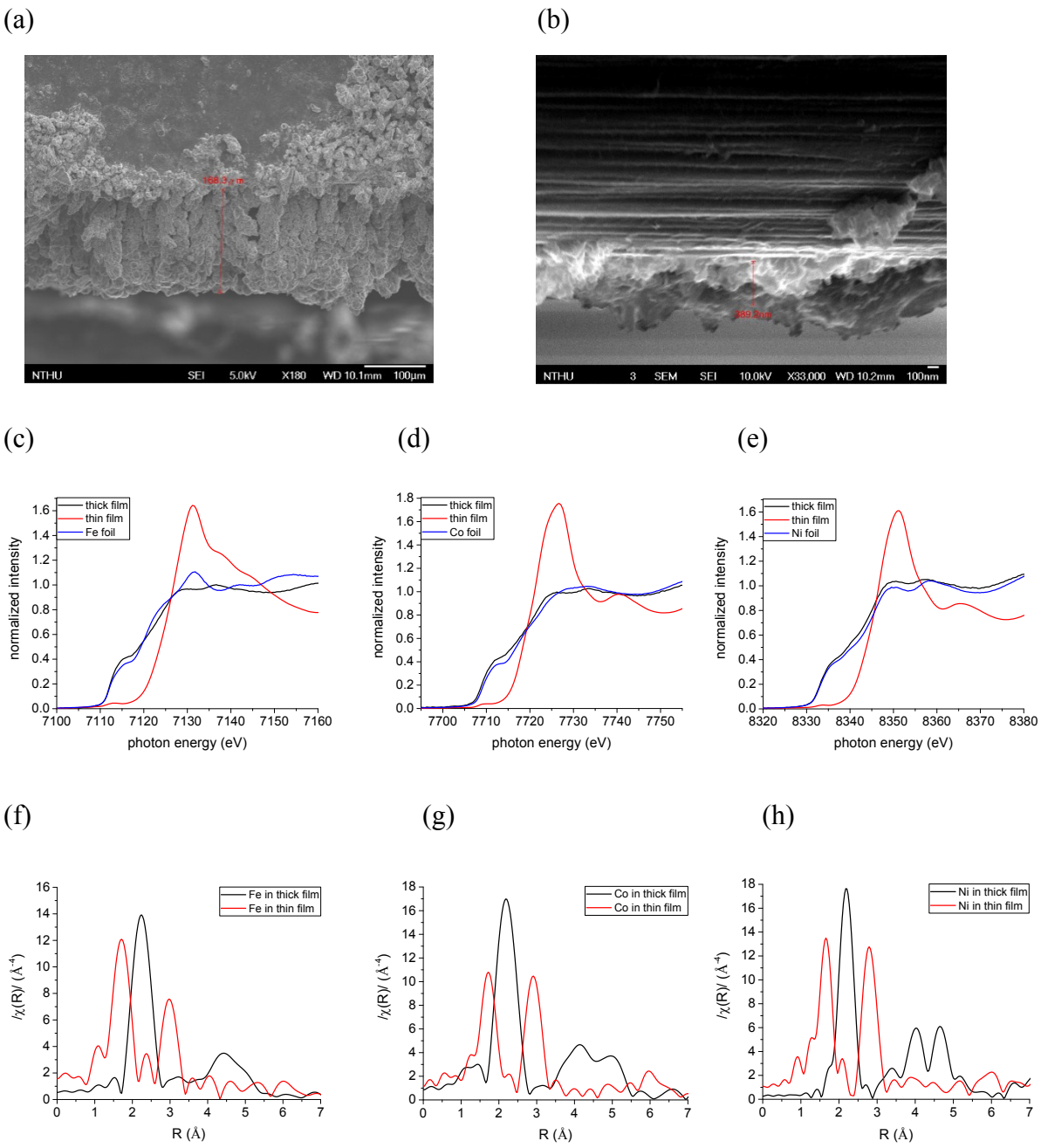

Figure S20. Cross-sectional SEM images of CFeCoNiP electrode. (a) thick film, and (b) thin film. The XANES spectra of (c) Fe K edge, (d) Co K edge, and (e) Ni K edge. The R-space EXAFS spectra of (f) Fe K edge, (g) Co K edge, and (h) Ni K edge.

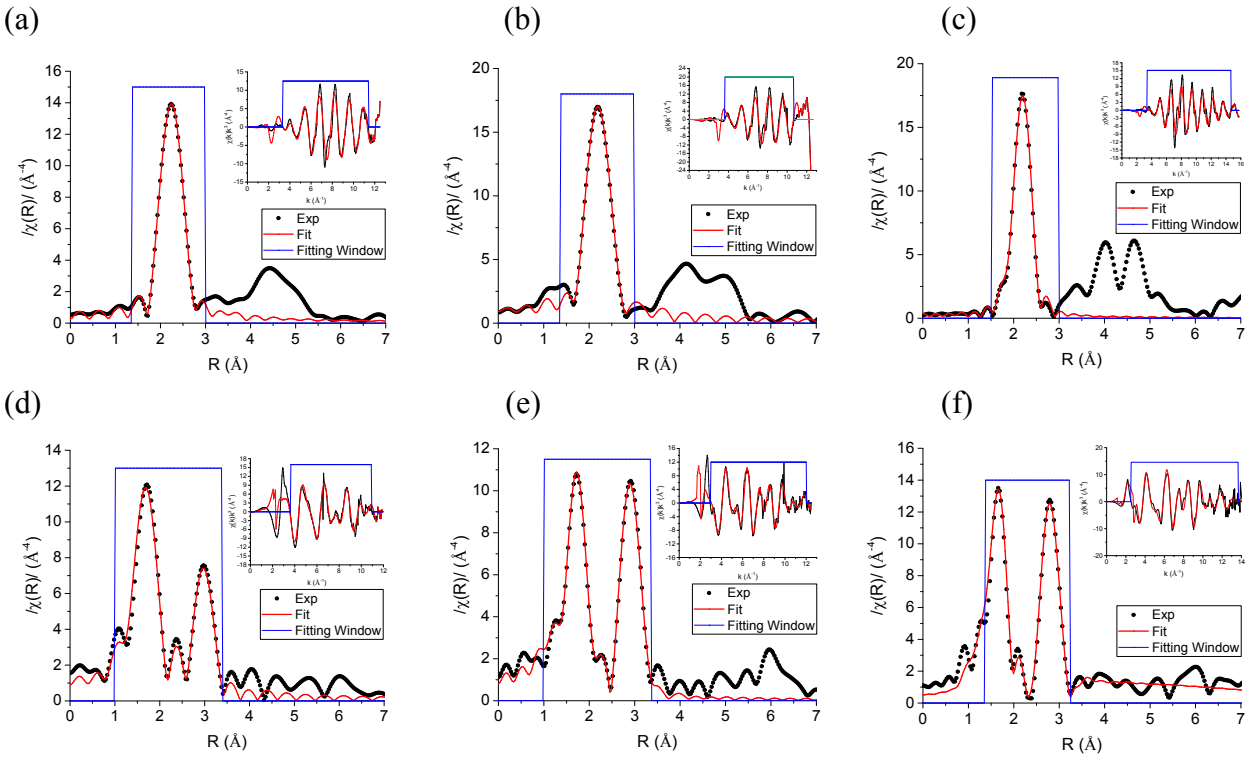

Figure S21. The k-space and R-space EXAFS spectra of thick film (a) Fe K edge, (b) Co K edge, (c) Ni K edge, and thin film (d) Fe K edge, (e) Co K edge, (f) Ni K edge. Shown are data (black) and fitting curves (red) within fitting window (blue). The detailed EXAFS fitting results are described in Tables S6 and S7.

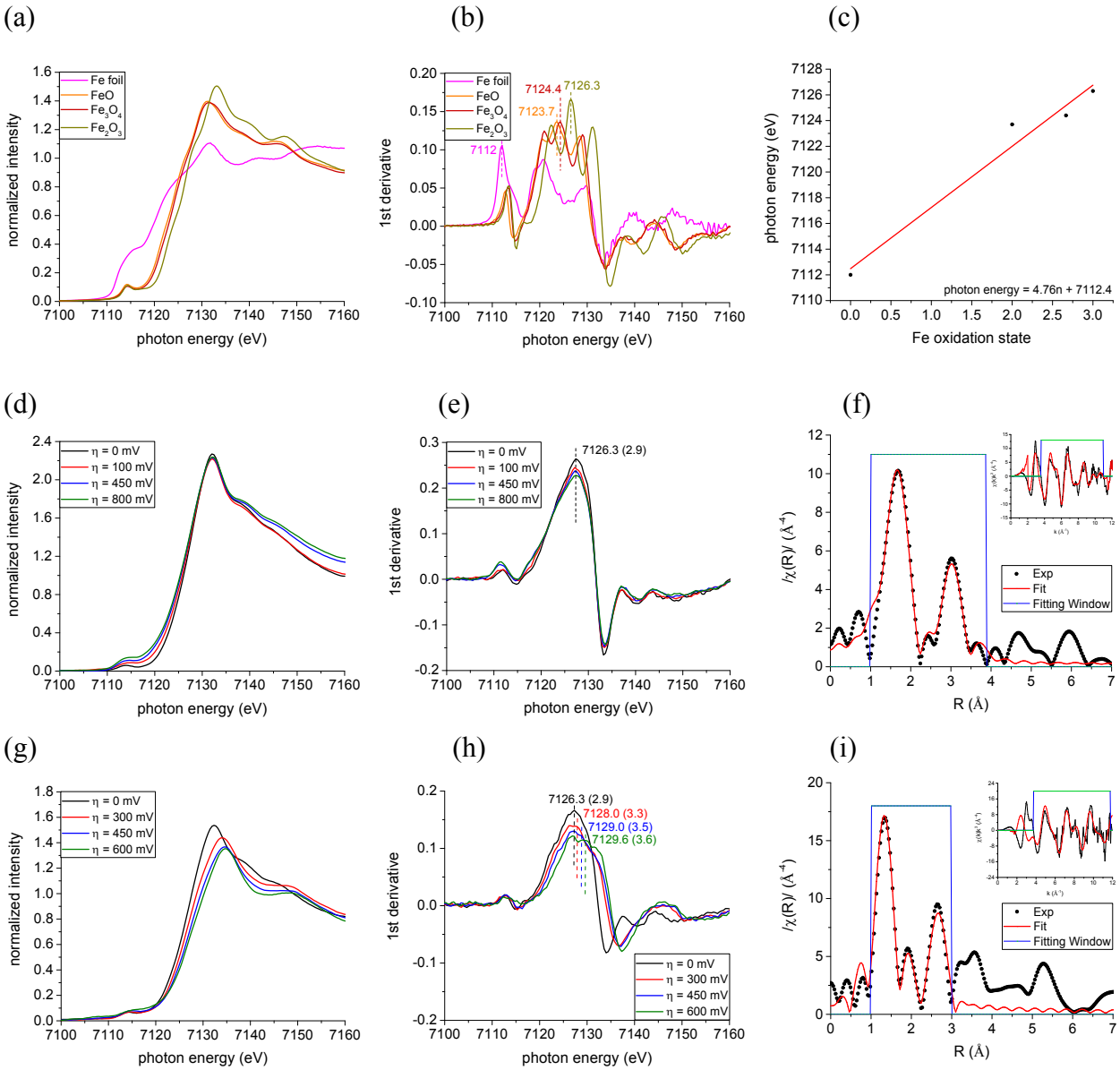

Figure S22. (a) The XANES and (b) the energy positions of the first derivative of XANES of Fe foil, FeO, Fe_3O_4 and Fe_2O_3, which were used as Fe^0, Fe^{2+}, $Fe^{2.67+}$ and Fe^{3+} references, respectively. (c) The linear regression follows the equation, photon energy = 4.76 (Fe oxidation state) +7112.4. The changes in Fe oxidation state under operational conditions are estimated by the equation. (d) Operando Fe K edge XANES and (e) the corresponding first derivatives under HER catalytic condition. (f) The k-space and R-space EXAFS spectra under HER overpotential of 800 mV. (g) Operando Fe K edge XANES and (h) the corresponding first derivatives under OER catalytic condition. (i) The k-space and R-space EXAFS spectra under OER overpotential of 600 mV. Shown are data (black) and fitting curves (red) within fitting window (blue). The detailed EXAFS fitting results are described in Table S7.

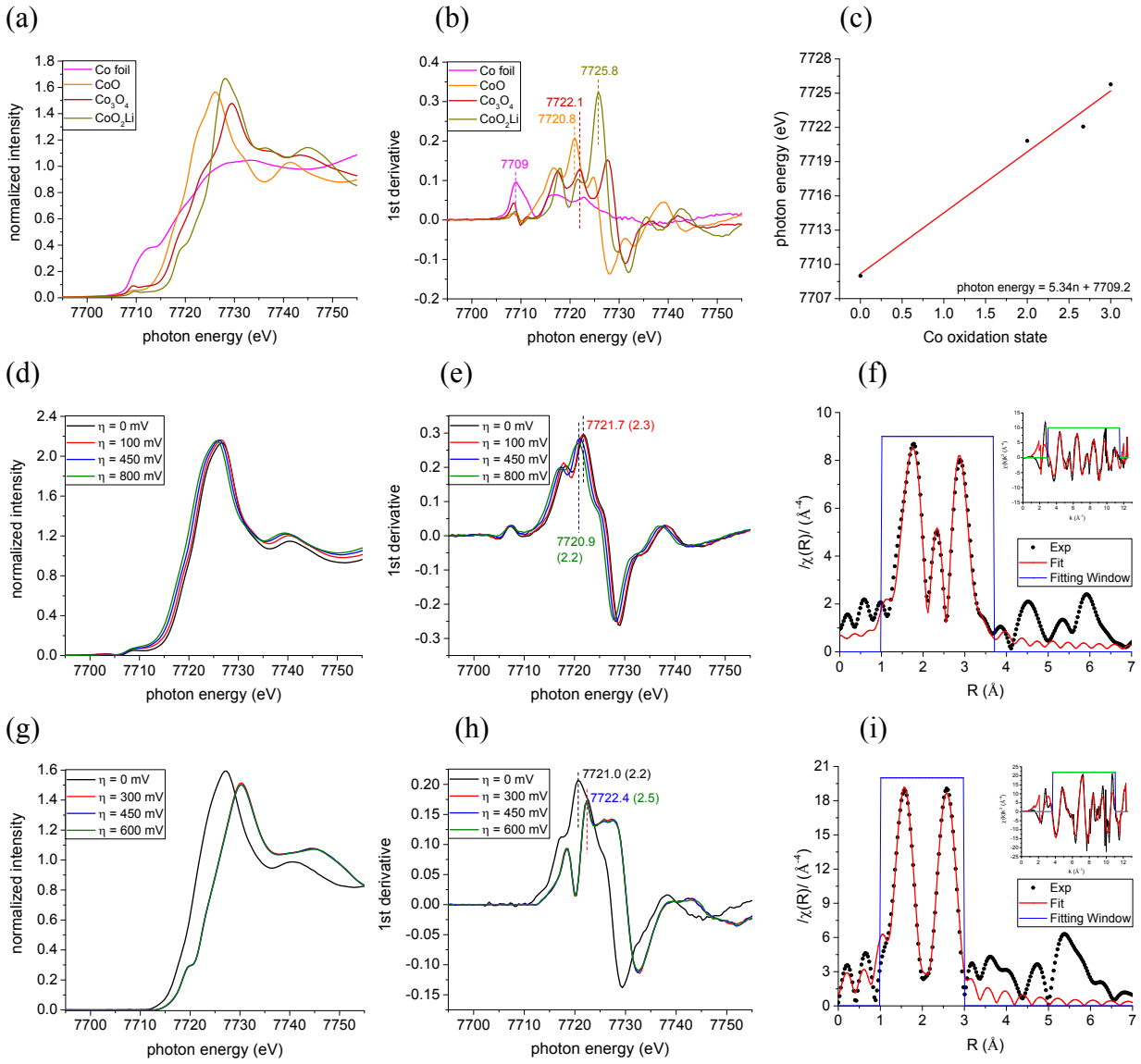

Figure S23. (a) The XANES and (b) the energy positions of the first derivative of XANES of Co foil, CoO, Co_3O_4 and CoO_2Li, which were used as Co^0, Co^{2+}, $Co^{2.67+}$ and Co^{3+} references, respectively. (c) The linear regression follows the equation, photon energy = 5.34 (Co oxidation state) + 7709.2. The changes in Co oxidation state under operational conditions are estimated by the equation. (d) Operando Co K edge XANES and (e) the corresponding first derivatives under HER catalytic condition. (f) The k-space and R-space EXAFS spectra under HER overpotential of 800 mV. (g) Operando Co K edge XANES and (h) the corresponding first derivatives under OER catalytic condition. (i) The k-space and R-space EXAFS spectra under OER overpotential of 600 mV. Shown are data (black) and fitting curves (red) within fitting window (blue). The detailed EXAFS fitting results are described in Table S7.

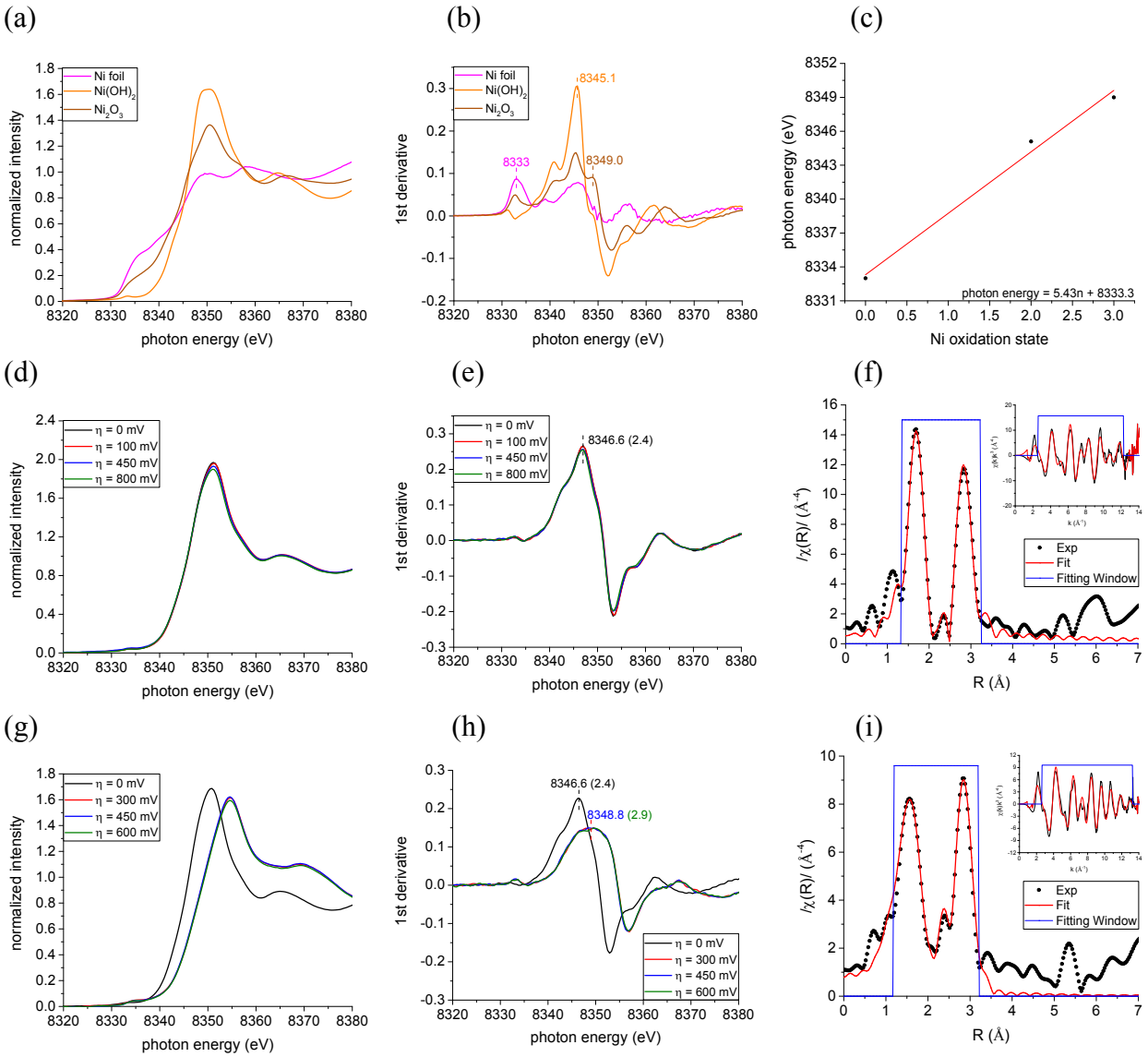

Figure S24. (a) The XANES and (b) the energy positions of the first derivative of XANES of Ni foil, $Ni(OH)_2$, and Ni_2O_3, which were used as Ni^0, $Ni^{2+}$and Ni^{3+} references, respectively. (c) The linear regression follows the equation, photon energy = 5.43 (Ni oxidation state) + 8333.3. The changes in Ni oxidation state under operational conditions are estimated by the equation. (d) Operando Ni K edge XANES and (e) the corresponding first derivatives under HER catalytic condition. (f) The k-space and R-space EXAFS spectra under HER overpotential of 800 mV. (g) Operando Ni K edge XANES and (h) the corresponding first derivatives under OER catalytic condition. (i) The k-space and R-space EXAFS spectra under OER overpotential of 600 mV. Shown are data (black) and fitting curves (red) within fitting window (blue). The detailed EXAFS fitting results are described in Table S7.

(a) (b)

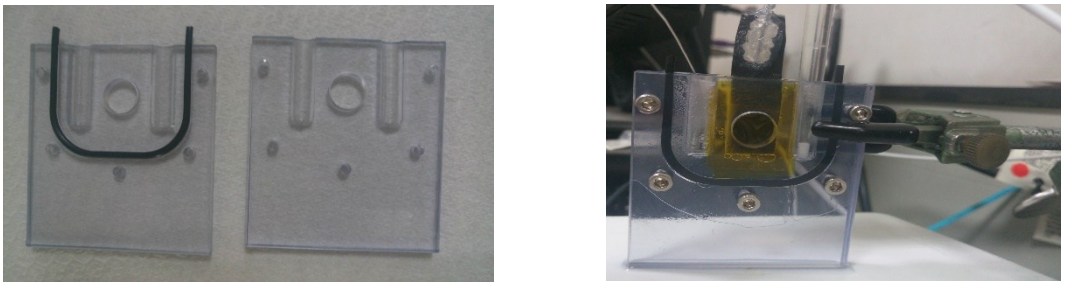

Figure S25. Pictures of in operando cell in electrochemical three-electrode operation. (a) The cell consists of three parts, including bottom part, top part and U-shape ring. (b) Because the X-ray beam generally propagates horizontally, the cell was placed vertically with the back of main electrochemical compartment facing toward the incoming beam. The main electrochemical compartment is formed by the central hole which is confined by two Kapton tapes, which serves as the window for X-ray beam.

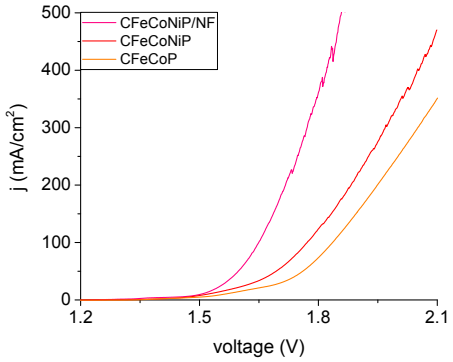

Figure S26. Polarization curve for overall water splitting of CFeCoNiP/NF-CFeCoNiP/NF electrode-pair setting shows the high current density performance in 1 M NaOH aqueous solution.

(a) (b)

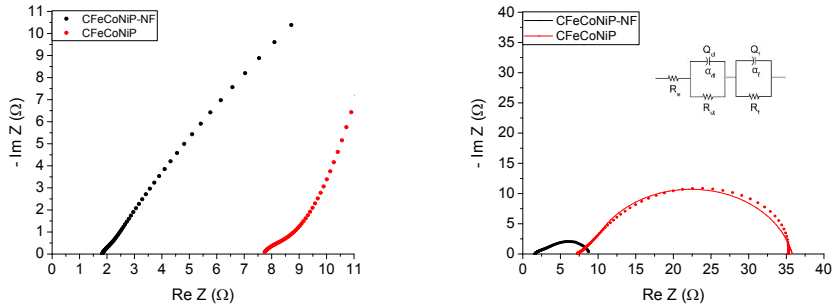

Figure S27. EIS measurements for overall water splitting using CFeCoNiP-CFeCoNiP and CFeCoNiP/NF-CFeCoNiP/NF electrode-pair settings. (a) Nyquist plots under OCP condition. (b) Nyquist plots at cell voltage of 1.58 V.

Table S1. Comparisons of HER performance for CFeCoNiP electrode with other reported electrocatalysts on carbon-based or metal-based support in 1 M alkaline electrolyte (KOH or NaOH). η_{10mA/cm^2} and η_{100mA/cm^2} correspond to the overpotentials at current densities of 10 and 100 mA/cm^2, respectively.

Electrocatalyst	Support	Tafel slope (mV/dec)	$\eta_{10\ mA/cm^2}$ (mV)	$\eta_{100\ mA/cm^2}$ (mV)	Reference
CFeCoNiP	graphite	36	37	174	This work
Pt-CoS_2 nanosheet	CC	82	24		Adv. Energy Mater. 2018, 8, 1800935
$NiCo_2P_x$ nanowires	CF	34.3	58	127	Adv. Mater. 2017, 29, 1605502
FLNPC@MoP-NC/MoP-C	CC	52	69		Adv. Funct. Mater. 2018, 28, 1801527.
porous FeCo-$NiSe_2$	CFC	89	92		Adv. Mater. 2018, 30, 1802121
O-CoMoS	CF	70	97		ACS Catal. 2018, 8, 4612
Ni/Mo_2C/porous C	GC	101	179	NA	Chem. Sci. 2017, 8, 968
Ni-P	CFC	85.4	117		Adv. Funct. Mater. 2016, 26, 4067.
Porous NiCoFe LTH	CFC	70	200		ACS Energy Lett. 2016, 1, 445
MoC/Mo_2C	GC	42	120	NA	Chem. Sci. 2016, 7, 3399
porous Mo_2C	GC	59	151	NA	Nat. Commun. 2015, 6, 1
CFeCoNiP/NF	NF	31	34	150	This work
MoO_2 nanosheets	NF	41	27		Adv. Mater. 2016, 28, 3785
V-Co_4N	NF	44	37		Angew. Chem. Int. Ed. 2018, 57, 5076
CoP-MNA	NF	51	54		Adv. Funct. Mater. 2015, 25, 7337
FeCoNi-HNTAs	NF	37.5	58		Nat. Commun. 2018, 9, 2452
P-NiFe	NF	67	75	NA	Chem. Sci. 2018, 9, 1375
$Co(OH)_2$@PANI	NF	91.6	88		Adv. Funct. Mater. 2015, 25, 6814
mesoporous FeS_2	NF	78	96	NA	J. Am. Chem. Soc. 2017, 139, 13604

Abbreviations: CC, carbon cloth; CF, carbon fiber; CFC, carbon fiber cloth; GC, glassy carbon; NF, Ni foam; FLNPC, few layered N, P dual doped carbon; LTH, layered triple hydroxide; MNA, mesoporous nanorod arrays; HNTA, hybrid nanotube arrays.

Table S2. Comparisons of OER performance for CFeCoNiP electrode with other reported electrocatalysts on carbon-based or metal-based support in 1 M alkaline electrolyte (KOH or NaOH). η_{10mA/cm^2} and η_{100mA/cm^2} correspond to the overpotentials at current densities of 10 and 100 mA/cm^2, respectively.

Electrocatalyst	Support	Tafel slope (mV/dec)	$\eta_{10\ mA/cm^2}$ (mV)	$\eta_{100\ mA/cm^2}$ (mV)	Reference number
CFeCoNiP	graphite	38	250	300	This work
defective EG NiFe LDH	GC	52	210		Adv. Mater. 2017, 29, 1700017
CoSe/NiFe LDH	EG	57	NA	270(150 mA/cm^2)	Energy Environ. Sci. 2016, 9, 478
$NiFeO_x$	CF	31.5	230	260	Nat. Commun. 2015, 6, 1
P-$CoSe_2$/N-C flake arrays	CC	36	230		Adv. Funct. Mater. 2018, 28, 1804846
porous FeCoNi LTH	CFC	32	239		ACS Energy Lett. 2016, 1, 445
N_2-CoS_2-400	CP	115	240	410(400 mA/cm^2)	ACS Catal. 2017, 7, 4214
porous FeCo-$NiSe_2$	CFC	63	251		Adv. Mater. 2018, 30, 1802121
CoAl-LDH	GC	36	252		Adv. Mater. 2016, 28, 7640
Co_4N	CC	44	257		Angew. Chem. Int. Ed. 2015, 54, 14710
FeCoOOH	CFC	30	266		Angew. Chem. Int. Ed. 2018, 57, 2672
Ni-Co nanowire	CF	43.6	302		Adv. Energy Mater. 2017, 7, 1601492
CoS/carbon nanotube	CP	72	306		ACS Nano 2016, 10, 2342
NiCoP@C	GC	96	330		Angew. Chem. Int. Ed. 2017,56, 3897
CoMnP	GC	61	330		J. Am. Chem. Soc. 2016, 138, 4006
CFeCoNiP/NF	NF	34	266 (100 mA/cm^2)	340 (500 mA/cm^2)	This work
NiFeV LDH	NF	42	195 (20 mA/cm^2)	233	Adv. Energy Mater. 2018, 8, 1703341
FeCoNi-HNTAs	NF	49.9	184		Nat. Commun. 2018, 9, 2452
$Ni_xFe_{1-x}Se_2$-DO	NF	28	195		Nat. Commun. 2016, 7, 12324
$(Fe_xNi_{1-x})_2P$	NF	66	156	255 (500 mA/cm^2)	Nano Energy 2017, 38, 553
FeNiP-NP	NF	76	180		Adv. Mater. 2017, 29, 1704075
Cu@NiFe LDH	Cu foam	27.8	199		Energy Environ. Sci. 2017, 10, 1820

Abbreviations: CC, carbon cloth; CF, carbon fiber; CFC, carbon fiber cloth; GC, glassy carbon; EG, exfoliated graphene; NF, Ni foam; LTH, layered triple hydroxide; HNTA, hybrid nanotube arrays.

Table S3. Comparisons of water splitting activity for CFeCoNiP electrode with other reported bifunctional electrocatalysts on carbon-based or metal-based support in 1 M alkaline electrolyte (KOH or NaOH).

Electrocatalyst	Support	Tafel slope (mV/dec)	Current density (j, mA/cm^2)	Voltage at the corresponding j (V)	Reference number
CFeCoNiP	graphite	43	10	1.52	This work
			100	1.77	
			300	1.96	
porous FeCo-$NiSe_2$	CFC	NA	10	1.52	Adv. Mater. 2018, 30, 1802121
FeCoNi LTH	CFC	70	10	1.55	ACS Energy Lett. 2016, 1, 445
			20	1.63	
Pt-CoS_2nanosheet	CC	NA	10	1.55	Adv. Energy Mater. 2018, 8, 1800935
Co-N-P doped carbon	EG	NA	10	1.60	Adv. Mater. 2017, 29, 1604480
CFeCoNiP/NF	NF	31	10	1.47	This work
			100	1.65	
			500	1.86	
$FeCoNiP_{0.5}S_{0.5}$-$FeCoNiP_0S_1$	Ti foil	NA	10	1.46	ACS Catal. 2018, 8, 9926
			100	1.68	
defective EG NiFe LDH	NF	NA	20	1.50	Adv. Mater. 2017, 29, 1700017
P-NiFe	NF	NA	10	1.51	Chem. Sci. 2018, 9, 1375
$MoNi_4/MoO_2$-MoS_2/Ni_3S_2	NF		10	1.47	Nat. Commun. 2017, 8, 15437
			200	1.70	
Cu@NiFe LDH	Cu foam	NA	10	1.54	Energy Environ. Sci. 2017, 10, 1820
			100	1.69	
Janus Co/CoP	NF	NA	10	1.45	Adv. Energy Mater. 2017, 7, 1602355
			20	1.66	
FeCoNi-HNTAs	NF	NA	10	1.429	Nat. Commun. 2018, 9, 2452
MoS_2/Ni_3S_2	NF	NA	10	1.50	ACS Catal. 2017, 7, 2357
Fe doped CoP	Ti foil	NA	10	1.60	Adv. Mater. 2017, 29, 1602441
np-$(Co_{0.52}Fe_{0.48})_2P$	free-standing	NA	10	1.53	Energy Environ. Sci. 2016, 9, 2257
Porous MoO_2	NF	NA	10	1.53	Adv. Mater. 2016, 28, 3785
NiCoP	NF	NA	10	1.58	Nano Lett. 2016, 16,7718
			100	1.82	
Co-P	Cu foil	69	10	1.56	Angew. Chem. Int. Ed. 2015, 54, 6251
			100	1.744	

Abbreviations: CC, carbon cloth; CFC, carbon fiber cloth; EG, exfoliated graphene; NF, Ni foam; LTH, layered triple hydroxide; HNTA, hybrid nanotube arrays.

Table S4. Summary of mass activity (MA) of (Fe, Co, Ni)-based electrocatalysts in 1 M NaOH aqueous solution.

Electrode	Mass activity (A/g)
HER (η = 100 mV)	
CFeCoNiP	7.43
CFeCoP[a]	5.83
CFeNiP	1.77
CCoNiP	3.64
CFeP[a]	0.77
CCoP	1.10
CNiP	1.16
OER (η = 350 mV)	
CFeCoNiP	62.81
CFeCoP[a]	41.37
CFeNiP	54.02
CCoNiP	13.75
CFeP[a]	1.60
CCoP	6.33
CNiP	5.61

[a]*ACS Appl. Energy Mater.*, 2018, **1**, 5298–5307

Table S5. Elemental composition (atomic %) analysis of film electrodes by EDX.

Electrode	Fe (%)	Co (%)	Ni (%)	P (%)	O (%)	Na (%)
HER						
CFeCoNiP	25.8	30.0	27.3	0	15.1	1.8
Post-HER	25.4	25.1	24.6	0	21.8	3.1
CFeCoP[a]	36.1	49.0	0	0	14.9	0
CFeNiP	39.4	0	42.1	1.1	14.3	3.1
CCoNiP	0	36.2	30.9	3.6	24.4	4.9
OER						
CFeCoNiP	21.2	24.2	22.4	1.3	26.4	4.5
Post-OER	8.6	9.0	8.1	3.1	54.0	17.2
CFeCoP[a]	21.0	24.9	0	2.9	43.2	8.0
CFeNiP	28.3	0	30.5	3.6	31.2	6.4
CCoNiP	0	24.6	23.2	6.9	40.0	5.3

[a]*ACS Appl. Energy Mater.*, 2018, **1**, 5298–5307.

Table S6. Elemental composition (atomic %) analysis of electrode surface by XPS.

Electrode	Fe (%)	Co (%)	Ni (%)	P (%)	O (%)[a]	Na (%)
HER						
CFeCoNiP	9.8	11.0	10.9	4.6	60.4	3.3
Post-HER	9.0	9.5	9.7	0	71.8	0
OER						
CFeCoNiP	7.2	8.1	7.6	3.1	70.3	3.7
Post-OER	6.5	7.0	6.6	0	79.9	0

[a]Due to adventitious organic residues, phosphate and water in the surrounding, oxygen is always present on samples surface exposed to the atmosphere, and the quantitation of oxygen content in these samples without argon ion sputter cleaning is not accurate.

Table S7. EXAFS fitting results for FeCoNi-based thick film under OCP condition in 1 M NaOH aqueous electrolyte. Amplitude reduction factor (S_0^2) was fixed at 0.9. M is denoted as Fe, Co and Ni.

XAS metal K edges	Fe K edge	Co K edge	Ni K edge
	Fe-M	Co-M	Ni-M
OCP (η = 0 mV)			
C.N.	9.5±0.1	9.5±0.1	9.5±0.1
R (Å)	2.65±0.01	2.57±0.01	2.54±0.01
ΔE_0 (eV)	-6.6±0.3	2.5±0.4	-11.0±0.6
σ^2 (10^{-3}xÅ^2)	9.4±0.1	7.1±0.2	8.0±0.2
R factor	0.0006	0.0041	0.0020

Table S8. EXAFS fitting results for FeCoNi-based thin film under OCP and operational conditions (HER/OER) in 1 M NaOH aqueous electrolyte. Amplitude reduction factor (S_0^2) was fixed at 0.9. M is denoted as Fe, Co and Ni.

XAS metal K edges	Fe K edge		Co K edge		Ni K edge	
	Fe-O	Fe-M	Co-O	Co-M	Ni-O	Ni-M
OCP (η = 0 mV)						
C.N.	4.3±0.2	9.6±0.9	5.5±0.1	9.5±0.2	5.8±0.1	9.6±0.6
R (Å)	1.99±0.01	3.09±0.02	2.06±0.01	3.16±0.01	2.03±0.01	3.10±0.01
ΔE_0 (eV)	16.4±1.5	-6.9±2.7	15.6±1.3	-10.1±2.2	4.7±1.5	9.0±2.8
σ^2 (10^{-3}xÅ^2)	5.3±0.7	9.9±0.5	6.7±0.3	10.3±0.2	5.7±0.7	9.2±0.6
R factor	0.0131		0.0051		0.0114	
HER (η = 800 mV)						
C.N.	4.0±0.2	9.4±0.8	3.6±0.1	9.2±0.6	3.8±0.1	9.3±0.5
R (Å)	1.98±0.02	3.12±0.02	2.07±0.01	3.15±0.01	2.06±0.01	3.14±0.02
ΔE_0 (eV)	15.3±2.9	10.8±2.2	14.5±1.1	14.0±1.6	7.7±1.1	10.8±2.3
σ^2 (10^{-3}xÅ^2)	9.4±0.3	10.1±0.4	5.2±0.6	6.5±0.5	1.4±0.4	9.3±0.6
R factor	0.0186		0.0163		0.0115	
OER (η = 600 mV)						
C.N.	4.2±0.2	7.5±0.7	5.3±0.3	7.8±0.5	5.5±0.2	7.7±0.3
R (Å)	1.72±0.01	2.58±0.03	1.94±0.02	2.69±0.02	1.95±0.01	2.96±0.02
ΔE_0 (eV)	-5.4±1.1	10.6±3.2	14.1±3.0	-7.5±3.8	3.5±1.4	-10.7±2.1
σ^2(10^{-3}xÅ^2)	3.2±0.4	9.6±0.7	5.6±0.6	8.3±0.6	5.8±0.9	9.5±0.3
R factor	0.0154		0.0101		0.0117	

Table S9. R_c, R_f and R_{ct} values extracted from EIS spectra of CFeCoNiP-CFeCoNiP and CFeCoNiP/NF-CFeCoNiP/NF electrode-pair settings.

Electrode-pair	R_c (Ω)	R_f (Ω)	R_{ct} (Ω)
OCP condition			
CFeCoNiP-NF	1.8		
CFeCoNiP	7.7		
Overall Water Splitting (η = 350 mV)			
CFeCoNiP-NF	1.6	0.5	6.7
CFeCoNiP	7.5	1.1	27.1

References

1. E. J. Miola, S. D. de Souza, P. A. P. Nascente, M. Olzon-Dionysio, C. A. Olivieri and D. Spinelli, *Appl. Surf. Sci.*,1999, **144-145**, 272–277.

2. L. C. Gontijo, R. Machado, E. J. Miola, L. C. Casteletti and P. A. P. Nascente, *Surf. Coat. Technol.*, 2004, **183**, 10–17.

3. *Handbook of X-Ray Photoelectron Spectroscopy*, October 1992, Perkin-Elmer Corporation, Physical Electronics Division.

4. H. Zhou, F. Yu, J. Sun, R. He, S. Chen, C.-W. Chu and Z. Ren, *Proc. Natl. Acad. Sci. U. S. A.*, 2017, **114**, 5607–5611.

5. C. C. L. McCrory, S. Jung, J. C. Peters and T. F. Jaramillo, *J. Am. Chem. Soc.*, 2013, **135**, 16977–16987.

6. C. C. L. McCrory, S. Jung, I. M. Ferrer, S. M. Chatman, J. C. Peters and T. F. Jaramillo, *J. Am. Chem. Soc.*, 2015,**137**, 4347–4357.

7. R. L. Doyle and M. E. G. Lyons, *Phys. Chem. Chem. Phys.*, 2013,**15**, 5224–5237.

8. X. Qian, T. Hang, S. Shanmugam and M. Li, *ACS Appl. Mater. Interfaces*, 2015, **7**, 15716–15725.

9. P. Chakthranont, J. Kibsgaard, A. Gallo, J. Park, M. Mitani, D. Sokaras, T. Kroll, R. Sinclair, M. B.

Mogensen and T. F. Jaramillo, *ACS Catal.*, 2017, **7**, 5399–5409.

10. H. Vrubel, T. Moehl, M. Grätzel and X. Hu, *Chem. Commun.*, 2013,**49**, 8985–8987.

11. S. Anantharaj, S. R. Ede, K. Karthick, S. S. Sankar, K. Sangeetha, P. E. Karthik and S. Kundu, *Energy Environ. Sci.*, 2018, **11**, 744–771.